

**DTIC FILE COPY**

4

AFGL-TR-88-0315

Application of the Theory of Wave  
Propagation Through Random Media  
To Phase and Amplitude Fluctuations  
of Seismic P-Waves

Stanley M. Flatte

University of California, Santa Cruz  
Department of Physics  
Santa Cruz, CA 95064

18 October 1988

Final Report  
18 February 1988-30 September 1988

DTIC  
ELECTE  
APR 25 1989  
S H D

APPROVED FOR PUBLIC RELEASE; DISTRIBUTION UNLIMITED

AIR FORCE GEOPHYSICS LABORATORY  
AIR FORCE SYSTEMS COMMAND  
UNITED STATES AIR FORCE  
HANSCOM AIR FORCE BASE, MASSACHUSETTS 01731-5000

AD-A207 207

089 4 25 129

Sponsored by:

DARPA Order No.

Monitored by:

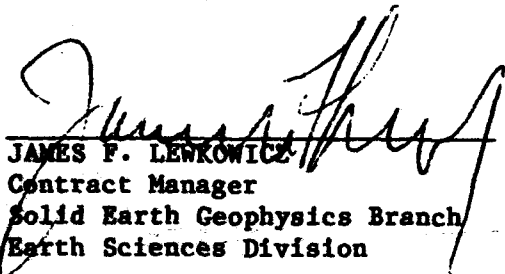
Contract No.:

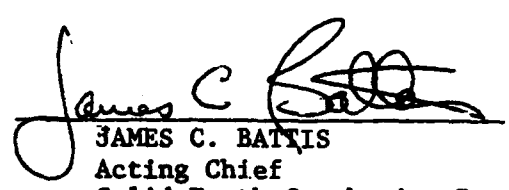
Defense Advanced Research Projects Agency  
Nuclear Monitoring Research Office  
5299

Air Force Geophysics Laboratory  
F19628-88-K-0014

The views and conclusions contained in this document are those of the authors and should not be interpreted as representing the official policies, either expressed or implied, of the Defense Advanced Research Projects Agency or the US Government.

"This technical report has been reviewed and is approved for publication"

  
JAMES F. LENKOWITZ  
Contract Manager  
Solid Earth Geophysics Branch  
Earth Sciences Division

  
JAMES C. BATTIS  
Acting Chief  
Solid Earth Geophysics Branch  
Earth Sciences Division

FOR THE COMMANDER

  
DONALD H. ECKHARDT, Director  
Earth Sciences Division

This document has been reviewed by the ESD Public Affairs Office (PA) and is releasable to the National Technical Information Service (NTIS).

Qualified requestors may obtain additional copies from the Defense Technical Information Center. All others should apply to the National Technical Information Service.

If your address has changed, or if you wish to be removed from the mailing list, or if the addressee is no longer employed by your organization, please notify AFGL/DAA, Hanscom AFB, MA 01731-5000. This will assist us in maintaining a current mailing list.

Do not return copies of this report unless contractual obligations or notices on a specific document requires that it be returned.

Unclassified

## SECURITY CLASSIFICATION OF THIS PAGE

REPORT DOCUMENTATION PAGE				Form Approved OMB No. 0704-0188	
1a. REPORT SECURITY CLASSIFICATION unclassified			1b. RESTRICTIVE MARKINGS		
2a. SECURITY CLASSIFICATION AUTHORITY			3. DISTRIBUTION/AVAILABILITY OF REPORT		
2b. DECLASSIFICATION/DOWNGRADING SCHEDULE			approved for public release; distribution unlimited		
4. PERFORMING ORGANIZATION REPORT NUMBER(S)			5. MONITORING ORGANIZATION REPORT NUMBER(S) AFGL-TR-88-0315		
6a. NAME OF PERFORMING ORGANIZATION The Regents of the University of California		6b. OFFICE SYMBOL (if applicable)		7a. NAME OF MONITORING ORGANIZATION Air Force Geophysics Laboratory	
6c. ADDRESS (City, State, and ZIP Code) University of California, Santa Cruz Santa Cruz, CA 95064			7b. ADDRESS (City, State, and ZIP Code) Hanscom AFB Massachusetts 01731-5000		
8a. NAME OF FUNDING/SPONSORING ORGANIZATION DARPA/Air Force		8b. OFFICE SYMBOL (if applicable)		9. PROCUREMENT INSTRUMENT IDENTIFICATION NUMBER F19628-88-K-0014	
8c. ADDRESS (City, State, and ZIP Code) Department of the Air Force Hanscom Air Force Base, MA 01731-5000			10. SOURCE OF FUNDING NUMBERS		
			PROGRAM ELEMENT NO. 61101E	PROJECT NO. 8A10	TASK NO. DA
			WORK UNIT ACCESSION NO. AB		
11. TITLE (Include Security Classification) Application of the Theory of Wave Propagation Through Random Media to Phase and Amplitude Fluctuations of Seismic P-Waves					
12. PERSONAL AUTHOR(S) Flatté, Stanley M.					
13a. TYPE OF REPORT Final		13b. TIME COVERED FROM 880218 TO 880930		14. DATE OF REPORT (Year, Month, Day) 881018	
15. PAGE COUNT 38					
16. SUPPLEMENTARY NOTATION					
17. COSATI CODES			18. SUBJECT TERMS (Continue on reverse if necessary and identify by block number)		
FIELD	GROUP	SUB-GROUP	Seismic waves, random media. (jbd)		
19. ABSTRACT (Continue on reverse if necessary and identify by block number)					
<p>Statistical descriptions of variations in P-wave velocity in the earth are related to observations in phase, travel-time, and amplitude fluctuations of seismic-wave signals received at teleseismic distances. A number of results have been obtained, including a model for variations down to 250 km under the NORSAR array in Norway, and for variations at a number of locations at the core-mantle boundary. Our final report consists of a list of articles published or submitted during the contract period, a short description of our objectives, a list of conferences attended, and copies of two reprints that give the essential technical content of our recent progress. <i>Keywords:</i></p>					
20. DISTRIBUTION/AVAILABILITY OF ABSTRACT <input checked="" type="checkbox"/> UNCLASSIFIED/UNLIMITED <input type="checkbox"/> SAME AS RPT. <input type="checkbox"/> DTIC USERS			21. ABSTRACT SECURITY CLASSIFICATION Unclassified		
22a. NAME OF RESPONSIBLE INDIVIDUAL James Lewkowicz			22b. TELEPHONE (Include Area Code) 617-377-3028		22c. OFFICE SYMBOL AFGL/LWH

**Final Technical Report for DARPA Contract F19628-88-K-0014**  
**(February 18 to September 30, 1988)**

This final technical report consists of a list of journal articles published wholly or in part under the auspices of the aforementioned contract, followed by a brief description of objectives, and a list of conferences attended by researchers supported by this contract. Copies of two journal articles that contain the main part of the technical progress made during this contract are appended.

1. J.M. Martin and S.M. Flatté, "Intensity images and statistics from numerical simulation of wave propagation in three-dimensional random media," *Applied Optics (Special Issue)*, vol. 27, pp. 2111-2126, June 1988.
2. S.M. Flatté and R.S. Wu, "Small-scale structure in the lithosphere and asthenosphere deduced from arrival-time and amplitude fluctuations at NORSAR," *J. Geophys. Res.*, vol. 93, pp. 6601-6614, June 1988.
3. K. Bataille and S.M. Flatté, "Inhomogeneities near the core-mantle boundary inferred from short-period scattered PKP waves recorded at the GDSN," *J. Geophys. Res.*, *in press*, December 1988.
4. T.F. Duda, S.M. Flatté, and D.B. Creamer, "Modelling meter-scale acoustic intensity fluctuations from oceanic fine structure and microstructure," *J. Geophys. Res.*, vol. 93, pp. 5130-5142, May 1988.
5. Lo T.W., M.N. Toksoz, S.H. Xu and R.S. Wu, 1988, Ultrasonic laboratory tests of geophysical tomographic reconstruction, *Geophysics*, 53, 947-956.
6. Wu, R.S. and K. Aki, 1988, Seismic wave scattering in the three-dimensionally heterogeneous earth, in the special issue "Seismic Wave Scattering and Attenuation", part I, ed. by Wu and Aki, *Pure and Applied Geophys.*, 128, 1-6.
7. Wu, R.S. and K. Aki, 1988, Multiple scattering and energy transfer of seismic waves, -separation of scattering effect from intrinsic attenuation. II. Application of the theory to Hindu Kush region, in the special issue "Seismic Wave Scattering and Attenuation", part I, ed. by Wu and Aki, *Pure and Applied Geophys.*, 128, 49-80.
8. Toksoz, M.N., A.M. Dainty, E.R. Reiter and R.S. Wu, 1988, A model for attenuation and scattering in the earth's crust, in the special issue "Seismic Wave Scattering and Attenuation", part I, ed. by Wu and Aki, 81-100.
9. Wu, R.S., 1988, On: "Stratigraphic filter theory: Combined effects of parallel bedding and random inhomogeneities" (I. Lerche), *Geophysics*, 53, 995-997.

10. Wu, R.S., 1988, Seismic wave scattering, invited article for the *"Encyclopedia of Geophysics"*, ed. by D. James, Van Nostrand Reinhold and Comp.
11. Wu R.S., 1988, Elastic wave scattering and the scalar wave approximation for seismic wave problems: The perturbation approach, submitted to the special issue *"Seismic Wave Scattering and Attenuation"*, part II, ed. by Wu and Aki, *Pure and Applied Geophys.*
12. Wu R.S., S.M. Flatte, 1988, Transmission fluctuations of seismic waves across seismic arrays, submitted to the special issue *"Seismic Wave Scattering and Attenuation"*, part II, ed. by Wu and Aki, *Pure and Applied Geophys.*
13. Bataille, K., R.S. Wu and S.M. Flatte, 1988, Inhomogeneities near the core-mantle boundary evidenced from seismic wave scattering. - a review, submitted to the special issue *"Seismic Wave Scattering and Attenuation"*, part II, ed. by Wu and Aki, *Pure and Applied Geophys.*
14. Turpening, R., C. Blackway and R.S. Wu, 1988, Differential vertical seismic profiles: Fracture volume analysis. submitted to *Geophysics*.
15. Keho, T. and R.S. Wu, 1988, Elastic Kirchhoff migration for vertical seismic profiling, submitted to *Geophysics*.
16. Wu, R.S., 1988, Representation integrals for elastic wave propagation containing either the displacement term or the stress term alone, submitted to *Phys. Rev. Letters*.

### Objective

The long-term objective of this work is to develop a quantitative understanding of the fluctuations in phase and amplitude of seismic wave propagation due to kilometer-scale variations in wave velocity within the earth. The theoretical approach is to describe these variations in a statistical way: in particular to consider the variations as represented by a spectrum that depends on depth, and may depend on geographical location. Data that are relevant to this approach include wave-forms with frequency content above one Hertz received on seismic arrays or on world-wide networks. Relatively high-frequency data is desirable because the ability to discriminate small structure is dependent on the wave having relatively short wavelength. Seismic arrays whose elements are spaced in the kilometers to tens-of-kilometers regime provide analysing power in that regime. Arrays with larger spacing, such as world-wide networks, can still probe small scales if the various available sources have separations in the above range; this can occur for earthquakes in active regions, or for nuclear explosions distributed within test sites.

A realistic understanding of the small-scale structure in the earth is important to fundamental geophysics because it affects our understanding of the fundamental dynamical processes in the earth. Mantle convection, chemical differentiation, fluid permeation, subduction-zone dynamics, and crack formation all will have their effects on small-scale structure, so that creation of more sophisticated theories of these processes will influence, and will be influenced by, our understanding of small-scale structure.

It is not likely that the seismological community will ever have a complete map of inhomogeneities in the earth down to kilometer scales. Therefore we will not be able to completely predict travel-time and amplitude fluctuations for a source-receiver geometry that is even a few kilometers different from previously measured situations. If we have a realistic statistical picture of the small-scale structure in wave-speed within the earth, then the theory of wave propagation through random media (WPRM) can be used to predict the scale and strength of travel-time and amplitude fluctuations due to earth structure. This information can then be used to calculate the accuracy of yield estimates and detection thresholds based on seismic information from an arbitrary array of seismometers, with *a priori* knowledge of results from nearby explosions or earthquakes. Furthermore, this knowledge can be used to design arrays in an optimal fashion to deal with random earth structure.

#### Conferences attended

The principal investigator attended the following meetings during the contract period:

Acoustical Society of America Meeting in Seattle, May, 1988. A talk on supercomputer simulation of wave propagation was given.

Massachusetts Institute of Technology, talk, June, 1988. A talk on supercomputer numerical simulation, and applications to seismology was given.

Jason summer study, July 1-31, 1988. The principal investigator led a sub-group investigation of regional wave propagation analysis.

Workshop on Wave Propagation in Random Media, in Tallin, Estonia, USSR, September 19-23, 1988. A talk on supercomputer simulation of wave propagation was given.

Institute of Atmospheric Sciences, Moscow, September 26, 1988. Discussions with Academician Obukhov and Professor V.I. Tatarskii were carried out. Their interests include general wave propagation in random media.

Lebedev Institute of General Physics, Moscow, September 26, 1988. Discussions with Drs. Bunkin,



For	
G&I	<input checked="" type="checkbox"/>
ad	<input type="checkbox"/>
tion	<input type="checkbox"/>
ion/	
ity Codes	
1 and/or	
Dist	Special

Dist

Special

A-1

Shishov, and Kravtsov were carried out. Their interests include the use of the theory of wave propagation in random media in ocean-acoustic applications.

Dr. Jan Martin attended a meeting of IUGG (the International Union of Geodesy and Geophysics) in Vancouver, Canada, August 9-22, 1988, where he gave a talk and discussed the use of the theory of wave propagation in random media in plasma physics applications.

# Inhomogeneities Near the Core-Mantle Boundary Inferred from Short-Period Scattered *PKP* Waves Recorded at the Global Digital Seismograph Network

KLAUS BATAILLE AND STANLEY M. FLATTÉ

*Physics Department and Institute of Tectonics, University of California, Santa Cruz*

We analyze short-period *PKP* precursor wave trains recorded at Global Digital Seismograph Network stations in the distance range  $120^\circ < \Delta < 140^\circ$  to infer the nature of inhomogeneities near the core-mantle boundary. Travel times and particle motions are consistent with predictions of single-scattered waves near the CMB. The dominant frequencies are around 1 Hz. The regions best sampled are beneath Indonesia, North America, Central Africa, and South America. Based on first-order scattering theory, the characteristics of the wave number spectrum of the structural inhomogeneities are obtained for two hypotheses: volume inhomogeneities and topographic irregularities. For the range of wavelengths sampled by these data (between 10 and 70 km), the spectrum of inhomogeneities is best represented by a power law of index 5.3 for volume inhomogeneities and 6.8 for topographic irregularities. If the scattering is due only to volumetric inhomogeneities, we estimate the strength of the structural variations to be about 0.5% in *P* wave velocity for a 200-km-thick layer. If the scattering is due only to topographic irregularities, the topography has an rms height of 280 m. At present we can not distinguish between these two types of inhomogeneities.

## 1. INTRODUCTION

There is increasing evidence for the existence of heterogeneities near the core-mantle boundary (CMB) which span wavelengths from approximately 10 to 3000 km. The upper limit of these wavelengths is intrinsically constrained by the size of the core, and the lower limit is observationally constrained by the probing wavelength of seismic waves. Although the evidence for heterogeneities is well established, there is still considerable debate about its physical nature. Among the proposed models for the nature of inhomogeneities are (1) thermal boundary layer, (2) chemical boundary layer, and (3) topographic irregularities. Currently, it is not possible to rule out any of these models from seismological observations alone.

There is agreement that the temperature difference between the top of D" and the CMB is at least 1000°K [Stacey and Loper, 1983; Jeanloz and Richter, 1979]; therefore a thermal boundary layer must be developed. Yuen and Peltier [1980] suggested that the thermal boundary layer is unstable and hence dynamically active, and not just the edge of a convective cell. Stacey and Loper [1983] suggested a mechanism for how mantle plumes originate at the bottom of the mantle, providing a solution of the temperature distribution within D" near the plume. This solution is consistent with observations of long-period core-diffracted waves [Doornbos et al., 1986]. Attempts at numerical simulation of this high-Rayleigh number convection situation are being made now (e.g., Boss and Sacks [1985] and Olson et al. [1987a, b] among others), as well as laboratory experiments [e.g., Loper and McCartney, 1986].

Two models of chemical boundary layers are proposed. First, due to the large density contrast between the core and the mantle, materials with densities smaller than the core and larger than the mantle would remain at the CMB [Ringwood, 1979].

Second, based on the phase diagram of FeO at high pressures and temperatures, Knittle and Jeanloz [1986] have suggested that the metallic iron core reacts chemically with the oxygen of mantle silicates, with the mantle residuum of such a reaction corresponding to the D' layer.

Among the seismological evidence for the presence of inhomogeneities, Ritzwoller et al. [1986] find indications of large-scale inhomogeneities in the core or lower mantle from anomalous splitting of eigenfrequencies associated with *PKP*, *SKS*, and *PKIKP*. Poupinet et al. [1983], Morelli and Dziewonski [1987], and Creager and Jordan [1986] also provide evidence of large-scale inhomogeneities near the CMB from inversion of travel times of *PKP* (BC and DF) phases for thousands of earthquakes. Different models for the structure near the CMB have been obtained from studies of waveforms and apparent slownesses of long-period core-diffracted *P* and *S* waves [Alexander and Phinney, 1966; Doornbos and Mondt, 1979; Mula and Müller, 1980] and *S*, *SKS*, and *ScS* waves [Mitchell and Helmberger, 1973; Lay and Helmberger, 1983; Schlüterhardt, et al. 1985], some with smooth variations, others with sharp discontinuities. Differences in the proposed models for the structure of D" might reflect its strong lateral variation. The effect of lateral variations on some of these phases is still debated [Comier, 1986].

Variability of small-scale heterogeneities can be tested by studying short-period *PKP* waves scattered at different locations worldwide. Haddon and Cleary [1974], King et al. [1974], Husebye et al. [1976], and others, presented clear evidence that the short-period wave train arriving before *PKIKP* originates from scattering by irregularities near the CMB. They based their evidence on studies of data from large seismic arrays. Although these authors find differences between regions sampled by their data, they agree that a few percent in density and seismic velocities in the lower mantle (D"), or a rough CMB with radial variations up to a few hundred meters could produce the observed energy level of precursors to *PKIKP* [Van der Berg et al., 1980]. Here we report on an analysis using available source-receiver geometries during a period of 6.5 years recorded at the

Copyright 1988 by the American Geophysical Union.

Paper number 88JB03196.  
0148-0227/88/88JB-03196\$05.00



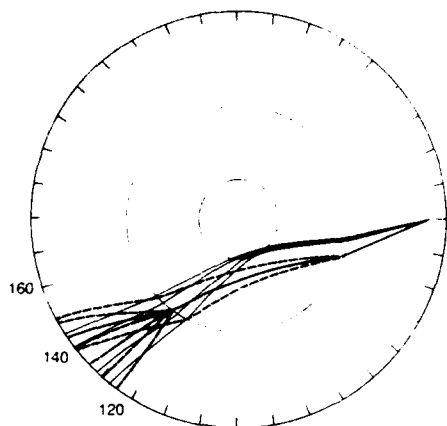


Fig. 1. Paths of *PKIKP* (thin solid curve), direct *PKP* (thick solid curve), and scattered *PKP* (thick dashed curve) at entrance and exit from the core arriving in the distance range  $120^\circ < \Delta < 150^\circ$ .

Global Digital Seismograph Network (GDSN). Our aim is to determine the nature of inhomogeneities for each region sampled. In section 2 we present the data and their characteristics; in section 3 we compare the data with the predictions of two scattering models: volumetric inhomogeneities and topographic irregularities; and in section 4 we discuss their relation and some geophysical implications.

## 2. DATA

Precursors to *PKIKP* in the distance range  $120^\circ < \Delta < 140^\circ$  recorded at the GDSN between 1980 and 1986 were analyzed. The paths of *PKIKP* and scattered *PKP* arriving as precursors are shown in Fig. 1. A rough estimate is that 200 events/year with magnitudes  $m_b > 5.7$  occur in the world. In principle, each of these events should have at least one GDSN station within the appropriate distance range for recording precursors. Thus, in

principle, a total of 1300 events are expected during the 6.5 years of data analyzed. Judged from their clear precursor signal, 130 records at 20 stations from 100 earthquakes were selected among available source-receiver paths.

Using data from large seismic arrays it is possible to determine the slowness of the arriving signal and distinguish in this way precursors (as scattered waves near the CMB) from noise. With a single-station method this is not possible. We distinguish precursor signals from noise based on three main criteria. First, to clearly identify the *PKIKP* arrival, events with sharp *PKIKP* onsets were selected. In general this is the case and only 5% of the total possible data set were discarded for this reason. Second, we compared the amplitude and frequency content of precursors with the noise background from more than 25 s before *PKIKP*. Amplitude of precursors above twice the noise background were selected; this accounted for about 85% of the selected set. For smaller amplitude ratios, we compared the frequency content; typically, precursors have a peak between 1 and 2 Hz while the noise has predominantly lower-frequency content; this criteria accounted for about 5% of the selected set. Third, the particle motion was examined when three-component records were available; only signals with steep angle of incidence were selected, which accounted for another 10% of the selected set. This third criterion is particularly useful for small distances where the amplitude of precursors could be as small as one fiftieth the amplitude of *PKIKP*. It will be shown later that the large number of events in the correct angular region that were not selected (because they showed no visible precursor) are also consistent with our model of CMB scattering, because our model predicts their precursor amplitude to be below the noise level. A more detailed description of the analysis and all the waveform data can be found in the work by Bataille [1987].

The regions of the CMB that are sampled by the data are shown in Fig. 2. The path between Indonesia and North America is better sampled due to the seismically active region in Indonesia and the good station coverage in North America.

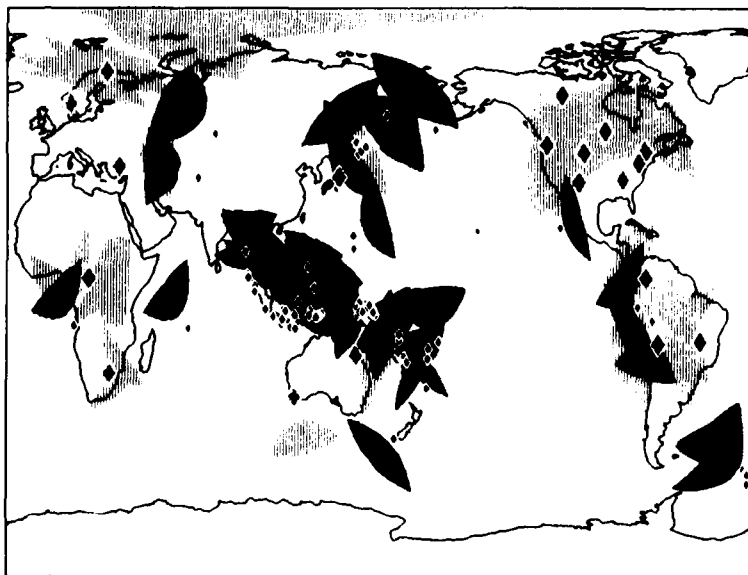


Fig. 2. Regions of the CMB sampled by the data. Dark (light) shaded regions represent scattering at the entrance (exit) of the core. Large light diamond represent receivers, and small dark diamonds represent sources.

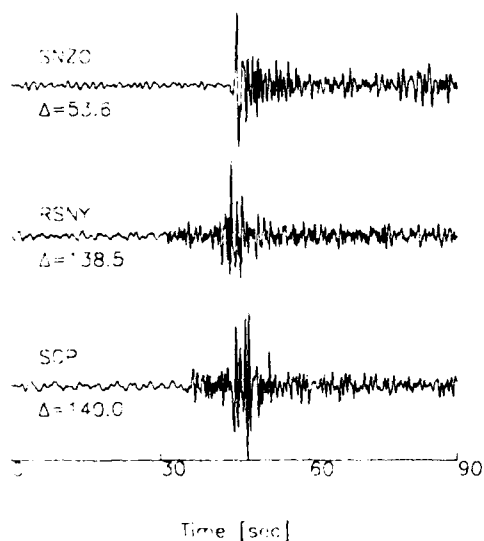


Fig. 3. An earthquake in Indonesia ( $9.4^{\circ}$  N,  $7.7^{\circ}$  W) recorded at a distance of  $53.6^{\circ}$  (SNZO) showing a simple  $P$  wave arrival, while at  $138.5^{\circ}$  (RSNY) and  $140^{\circ}$  (SCP) a clear precursor wave train is observed. The total display time is 90 s.

One typical example of the precursor wave train for one earthquake observed at different stations is shown in Fig. 3. The duration of the precursor and its uniform amplitude along the wave train are characteristics that can be explained by a scattering mechanism. For the event shown in Fig. 3, the station RSNY has three-component records available (Fig. 4(top)), and one can see from its particle motion diagram (Fig. 4(bottom)) that the incidence angles of precursor and of  $PKIKP$  do not differ by more than  $10^{\circ}$ . This small difference implies that precursors have passed through the CMB. Here we do not question further the origin of precursors and assume that all our data selected in this way are due to scattering near the CMB.

Variations of the properties of inhomogeneities from region to region would be manifested in variations of properties of the precursor wave train as recorded in different stations. Two properties of the precursor wave train can be compared: the complexity of the waveform, and its amplitude compared to  $PKIKP$ . All precursor wave trains have in general a continuous amplitude as a function of arrival time (see, for example, Figure 3); there are only 5% of these events with peaks localized in time. These peaks in amplitude might correspond to strong constructive interference among all scattered waves contributing at that particular time, or to a stronger inhomogeneity at a particular patch within the scattering region. With a single station it is not possible to resolve these two alternatives. We filter the  $PKIKP$  and precursor waveforms between 0.6 and 4 Hz using a Butterworth filter of first order. We do not find a systematic difference in the frequency content of the precursor signal as a function of epicentral distance, or as a function of geographical location. After filtering the  $PKIKP$  and precursor signal at the predominant frequency of  $PKIKP$ , we compute the amplitude of precursor/ $PKIKP$ , which as a function of distance is shown (for the stations with the most data points) in Fig. 5. All stations have a large scatter of data, in particular stations ZOBO and BCAA. This scatter could correspond to differences in the source geometry, source spectrum, or path. However, using the moment-tensor solution from the Harvard catalog, we compared the radiation pattern of  $PKIKP$  and their precursors, and varia-

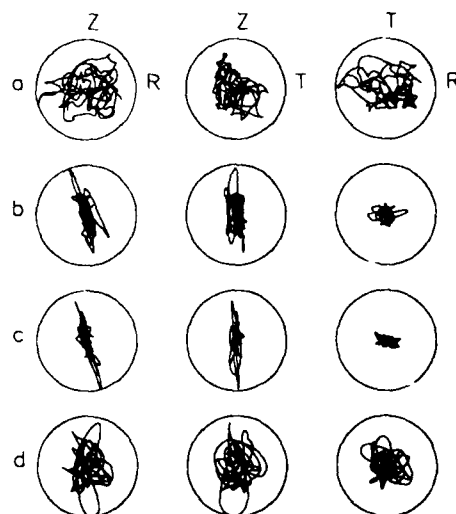
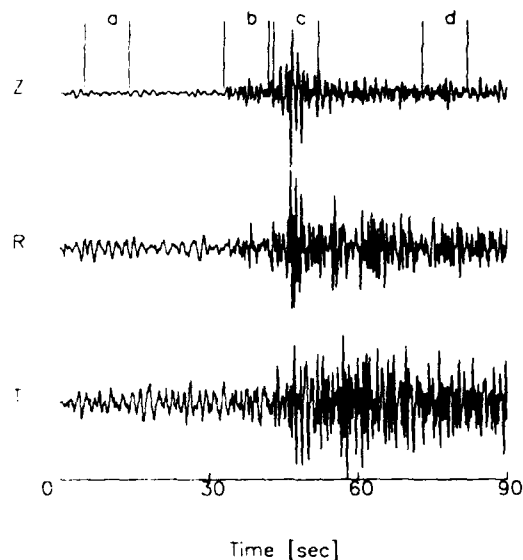


Fig. 4. (Top) Vertical (Z), radial (R), and transverse (T) component records at RSNY ( $\Delta = 138.5^{\circ}$ ). Note that the scales are not the same. (Bottom) Particle motion for four time windows: (a) noise preceding the precursor wavetrain, (b) precursor wavetrain, (c)  $PKIKP$ , and (d)  $PKIKP$ 's "coda."

tions in general were negligible. For the events during 1983 that were in the correct distance range, but that we did not select because no visible precursors were observed, we plotted the noise level during 1983 with a diamond symbol in Fig. 5. It can be seen for those cases that the noise level falls above the average level of scattered waves and therefore is consistent with our model of CMB scattering. There are two exceptions at station ZOBO, but that station has the largest scatter, and we see no inconsistency with our model. Although the data are limited, we find no systematic variation of the amplitude ratio at a given station as a function of azimuth. Also, the amplitude ratios at a given distance are equal for all stations within the scatter of the data. We have found no model of regional variation in the strength of inhomogeneities over the surface of the CMB that reduces the scatter in the data. We conclude that the spectral

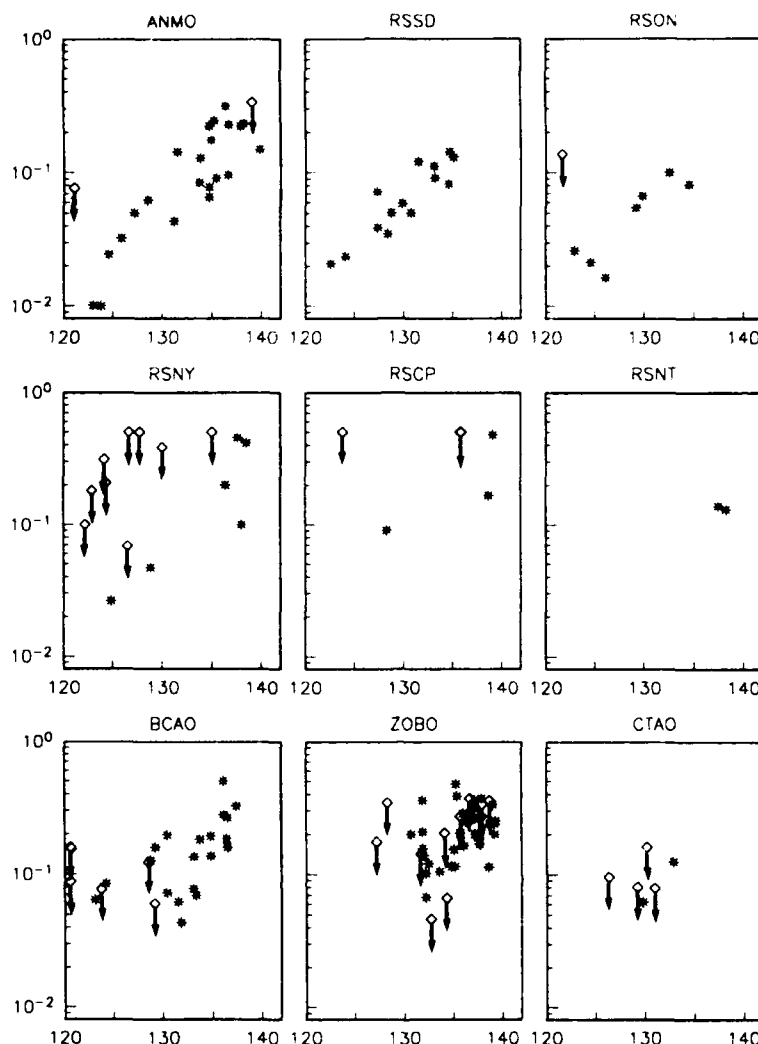


Fig. 5. Amplitude ratio of precursor/*PKIP* as a function of epicentral distance. The asterisks are calculated with events in which a precursor is observed. For events in which no precursor is identified, the diamond upper limits are calculated from the noise level during the precursor arrival time.

strength of the inhomogeneities is the same from region to region to within a factor of three. *Van den Berg et al.* [1980] measured the amplitudes of precursors recorded at 4 UKAEA arrays and NORSAR. Their observations of the ratio of precursor amplitude to *PKIP* at NORSAR and three of the UKAEA arrays are consistent with our results in Fig. 5. One of the arrays, YKA, shows consistently lower ratios, indicating less scattering. The data at YKA map the regions beneath the S. Sandwich Islands (at entrance) and Central North America (at exit), and all have an epicentral distance of about 136°. One tentative interpretation is to pinpoint the region beneath Central North America as less inhomogeneous compared to the other regions sampled, but more data is necessary to confirm this observation. In the next section we specify in more detail the implications that our observations have on the properties of inhomogeneities.

### 3. RESULT ANALYSIS

Our interpretation of precursors to *PKIP* is based on first-order scattering theory. In first-order theory each point of a

heterogeneous medium becomes a source of scattered waves of both *P* and *S* types. Only single-scattered waves are taken into account. A brief derivation of the formulas used below is presented in the appendix. The mean square amplitude of scattered waves can be expressed as

$$\langle |u|^2 \rangle = \frac{\pi}{4} k^4 \int_{CMB} A^2(x') R^2(x') \Omega(x') \Phi(K) d^2x' \quad (1)$$

where  $k$  is the wavenumber of the wave field,  $A$  is the product of the geometric spreading coefficient from the source to the scattering point and the geometric spreading coefficient from the scattering point to the receiver,  $R$  contains all the reflection/transmission coefficients and attenuation factors,  $K = k(\hat{n} - \hat{n}')$  where  $\hat{n}$  and  $\hat{n}'$  are the direction of the incident and scattered wave at the scattering point,  $\Phi(K)$  is the spectrum of inhomogeneities,  $\Omega = 1$  for volume inhomogeneities, and for topographic irregularities  $\Omega$  has a more complicated expression (see the appendix equation (A18)). Assuming  $\Theta$  to be the scattering angle, we have for volume inhomogeneities

$$\Phi^v(K) = \frac{H}{(2\pi)^3} \int \langle \delta\phi(x) \delta\phi(x+y) \rangle e^{iK \cdot y} d^3y \quad (2)$$

where

$$\delta\phi(x) = \frac{\delta\rho(x)}{\rho} \cos\Theta - \frac{\delta\lambda(x)}{\lambda + 2\mu} - \frac{2\delta\mu(x)}{\lambda + 2\mu} \cos^2\Theta \quad (3)$$

and  $H$  is the thickness of the inhomogeneous layer,  $\rho$  the density,  $\lambda$  and  $\mu$  the Lamé constants. For topographic irregularities

$$\Phi^t(K) = \frac{1}{(2\pi)^2} \int \langle \zeta(x) \zeta(x+y) \rangle e^{iK \cdot y} d^2y \quad (4)$$

where  $\zeta$  is the height of the interface with respect to the average.

In our model calculations we used the PREM structure [Dziewonski and Anderson, 1981] to compute travel time, geometric spreading, and attenuation. The PKP wave has a caustic near the CMB and ray theory predicts large amplitudes in its vicinity. We compute separately the contribution from both branches AB and BC, and neglect interference. Near the caustic we impose an amplitude cutoff equal to the amplitude one wavelength away from the cusp. Changing the cutoff amplitude to the amplitude two or three wavelengths away from the cusp did not appreciably affect the result, because the region where caustics develop is small compared to the total scattering region (several tens of wavelengths). The observability of precursors is not due to developing a caustic near the region of inhomogeneities; it is instead an effect of having a large scattering region at the CMB and of being the first arrivals at the station.

From studies of large seismic arrays [King et al., 1974; Doornbos, 1976] it was possible to determine for some cases the location of scattering, distinguishing scattering at entrance and exit from the core. For our data this is not possible and in our calculations we include both contributions, and neglect interference. If there are regions for which only scattering at entrance or exit contributes, we would underestimate the strength of such inhomogeneities by roughly one half.

For volume inhomogeneities, the mean square amplitude of the scattered waves depend on three independent random variables,  $\rho$ ,  $\lambda$ , and  $\mu$ . One could choose another set of independent random variables with more direct physical meaning, such as  $\rho$ ,  $\mu$ , and  $\kappa$  (compressibility);  $\rho$ ,  $\alpha$  ( $P$  wave velocity), and  $\beta$  ( $S$  wave velocity); or an easier seismological interpretation when  $\lambda = \mu$  by  $\alpha$  and  $\rho\alpha$  [Wu and Aki, 1985a]. In general, it is not possible to determine the characteristics of each variable independently. Even if  $\Phi(K)$  is known, it could be fitted by different combinations of strengths and correlations among these variables. However, if we consider  $P$  wave scattering in the forward direction, only one variable is involved:  $\alpha$ . Backscattered  $P$  waves depend on the  $P$  wave impedance,  $Z_p = \rho\alpha$ .  $P$  wave scattering at  $90^\circ$  angle depends on  $\lambda$  only. Choosing these three ( $\alpha$ ,  $Z_p$ , and  $\lambda$ ) as independent variables, (3) becomes

$$\delta\phi = -\frac{\delta\alpha}{\alpha}(\cos\Theta + \cos^2\Theta) + \frac{\delta Z_p}{Z_p}(\cos\Theta - \cos^2\Theta) - \frac{\delta\lambda}{\lambda + 2\mu}\sin^2\Theta \quad (5)$$

For precursors to PKIP the scattering angle varies roughly between  $10^\circ$  and  $50^\circ$ ; therefore we can neglect the contribution from fluctuations of  $P$  wave impedance. Furthermore, if the inhomogeneities are due to temperature, or compositional differences, leaving Poisson's ratio constant at  $\approx 0.25$ , such that we can approximate  $\mu = \lambda$ ,  $\delta\mu = \delta\lambda$ , we have

$$\delta\phi = -2\frac{\delta\alpha}{\alpha}(\cos^2\frac{\Theta}{2} - \frac{1}{3}\sin^2\Theta) \quad (6)$$

This is the relation we use to interpret volume inhomogeneities near the CMB. In the case of topographic irregularities, there is only one random variable involved: the height. From (1), (2), and (4) we have

$$\Phi^v(K) = \Omega\Phi^t(K) \quad (7)$$

and considering a thickness of 200 km for the inhomogeneous medium a correspondence between the variation of  $\alpha$  and the height  $\zeta$  is given approximately by

$$\zeta \approx 56\frac{\delta\alpha}{\alpha}(\text{km}) \quad (8)$$

The average scattering angle increases with decreasing epicentral distance. For a given epicentral distance the scattering angle varies by no more than about  $10^\circ$ . Typically, at a distance of  $140^\circ$  the average scattering angle is about  $10^\circ$ , and at  $125^\circ$  the average scattering angle is about  $50^\circ$ . If the spectral density of inhomogeneities corresponding to the scattering angle does not change significantly for variations of scattering angle of  $10^\circ$ , then  $\Phi(K)$  can be assumed constant. Taking the ratio of amplitudes of precursor / PKIP, from (1) we obtain

$$\Phi(K) = \frac{\langle |u|^2 \rangle^{\text{prec}}}{U^2} \bigg|_{\text{obs}} \frac{4(g^{\text{pkip}} R^{\text{pkip}})^2}{\pi k^4 A^2 R^2 \Omega dS} \bigg|_{\text{calc}} \quad (9)$$

where  $U|_{\text{obs}}$  is the observed amplitude of PKIP, and  $g^{\text{pkip}}$  and  $R^{\text{pkip}}$  are the geometric spreading and transmission coefficients relevant to PKIP calculated using ray theory. The effect of different proposed  $Q$ 's along the different paths through the mantle, outer, and inner core is negligible in this case. Fig. 6 shows the result of  $\Phi(K)$  for both (1) volumetric inhomogeneities and (2) topographic irregularities, for all stations. Comparing the results for different stations we find no evidence for regional variations of the strength of inhomogeneities of greater than a factor of three. The spectrum can be approximated as a power law by  $\Phi(K) = \Phi_0 |K|^{-p} (\text{km}^4)$ , with  $K$  in units of  $\text{km}^{-1}$  and  $\Phi_0 = (3.4 \pm 1.5) \times 10^{-6}$ ,  $(4.3 \pm 2.2) \times 10^{-7}$ , and  $p = 5.3 \pm 0.2$ ,  $6.8 \pm 0.3$ , for volumetric inhomogeneities and topographic irregularities, respectively. This is different from the Gaussian correlation used by Haddon and Cleary [1974] and

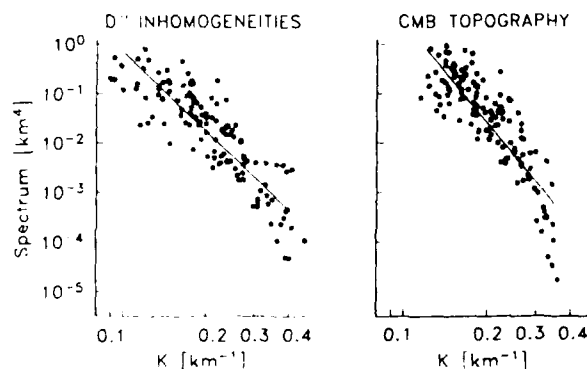


Fig. 6. Spectra  $\Phi (\text{km}^4)$  deduced from the data of Figure 5 under the assumption of (left)  $D''$  inhomogeneities and (right) CMB topography. The line represents the best fit power law which has index  $p = 5.3$  (left) and  $6.8$  (right). The spatial wave number  $|K| (\text{km}^{-1})$  refers to the inhomogeneities (assumed isotropic) or to the topographic features.

Doornbos [1976]. Recently Flatté and Wu [1988] inverted for the small-scale inhomogeneities beneath NORSAR, in Norway, and found that the heterogeneities below the lithosphere are best represented by a power law spectrum of index between 4 and 5.

#### 4. GEOPHYSICAL IMPLICATIONS

The total variance of the  $P$  wave velocity through  $D''$  and the height of the topography at the CMB are obtained from the integration of  $\Phi^{*j}(K)$  over the observed domain of wavelengths (10–70 km). The result for topographic irregularities is  $280 \pm 100$ -m *rms* height. This result is consistent with the estimate by Doornbos [1978] and the upper limit from Menke [1986] of topographic irregularities of a few hundred meters height. The result for three-dimensional heterogeneities is  $0.5 \pm 0.1\%$  for  $P$  wave velocity variations. It should be emphasized that our result determines the product of  $\delta\alpha^2 H$ , and we are assuming that  $H = 200$  km. Relating the variations of seismic velocities with temperature as  $\rho\delta\phi^* = a\delta T$ , with  $a = 2 \times 10^8 \text{ erg cm}^{-3} \text{ K}^{-1}$  (from Jones [1977]), where  $\phi^* = \alpha^2 - \frac{4}{3}\beta^2$ , and neglecting variations in pressure) we obtain  $\delta T \approx 700^\circ\text{K}$ . It is possible then that these heterogeneities have a thermal origin.

If the spectrum of the correlation function of topographic irregularities is valid for larger wavelengths, then one can predict the increase in mean square height expected from increasing the domain of integration. For instance, if we take scales up to 1000 km, the height is 23 km, which is somewhat more than Creager and Jordan [1986] suggest (5 km) for the height of the irregularities from analysis of PKP travel times. This suggests that the true spectrum lies below a simple extrapolation of our spectrum to wavelengths significantly above 70 km. It may be worthwhile to point out that mechanisms with characteristic scales of a few hundred kilometers could explain this behavior. For example, a statistical process with a characteristic scale and an exponential correlation function has a flat spectrum at long wavelengths and a  $K^{-4}$  spectrum at short wavelengths. Examples of such mechanisms could be convection cells, or the catchment area for plume material. Similar extrapolations for volume inhomogeneities are not possible without including anisotropy. It seems natural to consider the thickness of the  $D''$  layer as the upper limit for the scales where the inhomogeneities can be considered isotropic. This is approximately 3 times the upper limit of our analysis. Assuming that the spectrum of the correlation function of volumetric inhomogeneities is valid up to 200 km, a value of 2.5% for the  $P$  wave velocity variation is predicted. If this  $P$  wave variation has a thermal origin, variations in temperature would have to be  $\delta T \approx 3000^\circ\text{K}$ . New results from laboratory experiments have indicated that the temperature change across  $D''$  is about  $2000^\circ\text{K}$  [Knittle et al. 1987], so that a thermal origin for our observed  $P$  wave variations is possible. On the other hand, the derivative of  $P$  wave velocity with respect to temperature may be much less at higher pressure [Ahrens and Hager, 1987], which would require much larger temperature variations to explain our observations. We conclude that interpreting our results in terms of thermal variations alone would have to await the resolution of present uncertainties on the temperature change across  $D''$  and the relation of temperature change to  $P$  wave velocity change at high pressure.

It is also possible to associate our observed  $P$  wave velocity variations with chemical heterogeneity. This heterogeneity could arise from mixing between the iron core and mantle silicates, resulting in formation of mantle minerals such as FeO [Knittle et

al. 1987]. Since the  $P$  wave velocity of FeO alloys is expected to be substantially smaller than that of the mantle, this model would require very small inclusions contributing a variable but small mass fraction to a 200-km-thick  $D''$ . Other mechanisms include subducted crustal slabs [Ringwood, 1979; Olson et al. 1987 a, b] and primary chemical layering [Jordan and Creager, 1987].

#### 5. CONCLUSIONS

By analyzing the characteristics of precursors for all available source-receiver paths from GDSN data, we have shown that the spectrum of inhomogeneities satisfies a power law distribution of index  $5.3 \pm 0.2$  for volumetric inhomogeneities and  $6.8 \pm 0.3$  for topographic irregularities. These inhomogeneities correspond to variations of  $280 \pm 100$ -m *rms* height if scattering is due only to topography, or approximately  $0.5 \pm 0.1\%$  in  $P$  wave velocity if it is due only to volumetric inhomogeneities. At present, we can not distinguish between these two types of inhomogeneities. We find evidence for similarities of the properties of inhomogeneities ( $P$  wave speed variation in  $D''$  or *rms* height of CMB topography) between several different geographical regions within a factor of three in the strength of the inhomogeneity. It is possible at present to consider these variations as arising from either thermal or chemical heterogeneities, but this information, in combination with further constraints on material properties from laboratory experiments and progress in geodynamic simulations, will significantly limit allowable models of the core-mantle boundary region.

#### APPENDIX

Here we present briefly the theory of wave scattering in random media used in this study. Two cases are analyzed: scattering by volumetric inhomogeneities and topographic irregularities.

##### Volume Inhomogeneities

We use a theory developed by Chernov [1960] for acoustic waves and extended to elastic waves by Knopoff and Hudson [1964] and Wu and Aki [1985a, b]. This method was also used for studies of precursors to PKIKP by Haddon and Cleary [1974] and Doornbos [1976].

The equation of motion for a general inhomogeneous isotropic elastic medium is

$$\rho \frac{\partial^2}{\partial t^2} u(x, t) - \nabla \left[ \lambda \nabla \cdot u(x, t) \right] - \nabla \cdot \left\{ \mu \left[ \nabla u(s, t) + \nabla u(s, t)^T \right] \right\} = f(x, t) \quad (\text{A1})$$

or

$$Lu = f \quad (\text{A2})$$

where  $\rho$  is the density,  $\lambda$  and  $\mu$  are the Lamé constants,  $u$  is the displacement,  $f$  is the body force, and  $L$  a linear operator which depends on the parameters of the medium. For a radially symmetric Earth model,  $\rho_0$ ,  $\lambda_0$  and  $\mu_0$  vary smoothly with radius, and (A2) can be written as

$$L_0 u^{(0)} = f \quad (\text{A3})$$

with solutions given by

$$u^{(0)}(x, t) = \int G(x, x', t) * f(x', t) d^3x' \quad (\text{A4})$$

where the Green's function  $G(x, x', t)$  is obtained from ray theory [Aki and Richards, 1980], and  $*$  means convolution in time. In the presence of inhomogeneities such that  $\rho = \rho_0 + \delta\rho$ ,  $\lambda = \lambda_0 + \delta\lambda$ , and  $\mu = \mu_0 + \delta\mu$ , the equation of motion assuming no body forces becomes

$$L_0 u = Qu \quad (A5)$$

where

$$Q = \nabla(\delta\lambda \nabla \cdot) + \nabla \cdot \left[ \delta\mu(\nabla + \nabla^T) \right] - \delta\rho \frac{\partial^2}{\partial t^2} \quad (A6)$$

depends only on the inhomogeneities.

Decomposing  $u$  into the incident wave,  $u^{(0)}$ , plus the scattered wave,  $u^{(1)}$ , and assuming that  $|u^{(1)}| \ll |u^{(0)}|$  (Born approximation), the equation for the scattered wave is

$$L_0 u^{(1)} = Qu^{(0)} \quad (A7)$$

which has a solution

$$u^{(1)}(x, t) = \int G(x, x', t) * Qu^{(0)}(x', t) d^3x' \quad (A8)$$

To calculate the average intensity of the scattered  $P$  wave over all possible realizations of the random medium, we take the ensemble average of the square amplitude and, after some algebra, find

$$\langle |u^{(1)}|^2 \rangle = \frac{\pi}{4} k^4 \int C M B A^2(x') R^2 \Phi(K) d^2x' \quad (A9)$$

where  $k$  is the wave number of the wave field,  $A$  is the product of the geometric spreading coefficient from source to the scattering point and the geometric spreading coefficient from the scattering point to the receiver,  $R$  contains all the transmission/reflection coefficients and attenuation factors,  $K = k(\hat{n} - \hat{n}')$ , and  $\hat{n}$  and  $\hat{n}'$  are the direction of the incident and scattered wave at the scattering point. Assuming  $\Theta$  to be the scattering angle, and  $H$  the thickness of the inhomogeneous layer we have

$$\Phi(K) = \frac{H}{(2\pi)^3} \int \langle \delta\phi(x) \delta\phi(x+y) \rangle e^{iK \cdot y} d^3y \quad (A10a)$$

$$\delta\phi(x) = \frac{\delta\rho}{\rho} \cos\Theta - \frac{\delta\lambda}{\lambda + 2\mu} - \frac{2\delta\mu}{\lambda + 2\mu} \cos^2\Theta \quad (A10b)$$

From the analysed earthquakes which have magnitudes  $5.7 < m_b < 6.7$ , the duration of the  $PKIKP$  wave is between 4 and 8 s, and the dominant frequency is around 1 Hz. To model these characteristics we assumed a source of monochromatic waves with a frequency of 1 Hz and a Gaussian envelope of 4 s duration. Changing the source duration from 4 to 8 s does not affect the result appreciably.

### Topographic Irregularities

No exact theory of wave scattering for general rough surfaces is available. However, effective approximate methods have been developed for some cases. The small perturbation method which is valid for roughness with small heights and slopes was applied to elastic media by Kennett [1972] and used to study precursors to  $PKIKP$  by Doornbos [1978]. On the other hand, the Kirchhoff-Helmholtz method is valid for large heights with smooth slopes and was used in seismology by Scott and Helmburger [1983], who studied body wave reflections from mountains and spall from nuclear blasts; Frazer and Sen [1985] and Sen and Frazer [1985] used it to study reflections in a laterally inhomogeneous multilayered medium. Here we present a brief derivation of the Kirchhoff-Helmholtz method.

Let  $V$  be a volume and  $\partial V$  its boundary with outward pointing unit normal  $\hat{m}$ . Let  $f_1$  and  $f_2$  be some distribution of force densities, and let  $u_1, \tau_1, u_2$ , and  $\tau_2$  be the displacements and stresses due to  $f_1$  and  $f_2$  respectively. The equation of motion in the frequency domain is

$$-\rho\omega^2 u_i = \nabla \cdot \tau_i + f_i \quad (i = 1, 2) \quad (A11)$$

Integrating (11) with  $i = 1$  over a volume  $V$  after dot product with  $u_2$ , permuting indices and subtracting from each other, and using the divergence theorem, we obtain

$$\int_V (f_2 \cdot u_1 - f_1 \cdot u_2) dV = \int_{\partial V} \hat{m} \cdot (\tau_1 \cdot u_2 - \tau_2 \cdot u_1) dS \quad (A12)$$

Here  $f_1$  and  $f_2$  are in general arbitrary; by choosing  $f_1$  to be

nonzero outside of  $V$  and  $\partial V$ , and  $f_2 = \delta\delta(x - x_2)$  where  $x_2 \in V$ , we obtain

$$\hat{m} \cdot u_1(x_2) = \int_{\partial V} \hat{m} \cdot (\tau_1 \cdot u_2 - \tau_2 \cdot u_1) dS \quad (A13)$$

Considering a medium with a material discontinuity, the boundary  $\partial V$  is taken as a surface infinitely close to the material discontinuity from the receiver side. Using ray theory to calculate  $u_1, \tau_1, u_2$ , and  $\tau_2$ , the expression for the displacement, dropping the subscript 1, becomes

$$u = ik \int_{\Sigma} A R \gamma e^{i\omega T} dS \quad (A14)$$

where  $\Sigma$  is the illuminated surface of the CMB;  $A$  and  $R$  are the same as in (A9),  $T$  is the travel time, and  $\gamma$  depends on the slope of the interface and physical parameters of both media as follows:

$$\gamma = (C_p + \frac{P'S'}{P'P'} C_s) \cdot \hat{m} \quad (A15)$$

$$C_p = (\lambda - 2\mu \hat{n} \cdot \hat{n}')(\hat{n}' - \hat{n}),$$

$$C_s = (\frac{\alpha}{\beta} \mu \hat{s}' - 2\mu \hat{n}') \hat{s} \cdot \hat{n}' + \hat{s} (\frac{\alpha}{\beta} \mu \hat{s}' \cdot \hat{n}' - \lambda) \quad (A16)$$

where  $\hat{n}$  is the direction of the incident wave,  $\hat{n}'$ ,  $\hat{s}$ ,  $P'P'$  and  $P'S'$  are the directions of displacement and transmission coefficients of transmitted  $P$  and  $S$  waves, respectively, and  $\hat{s}'$  is the direction of propagation of the transmitted  $S$  wave satisfying  $\hat{s}' \cdot \hat{s} = 0$ .

Let  $\zeta(r)$  be the height of the interface with respect to the average. For small heights,  $A$  is considered independent of  $\zeta$ , and keeping only the first term of the expansion of  $R$  and  $\gamma$  in powers of  $\nabla\zeta$ , and  $T$  in powers of  $\zeta$ , the ensemble average of the square amplitude takes the form

$$\langle |u|^2 \rangle = \frac{\pi}{4} k^2 \int_{\Sigma} A^2 R^2 \left[ a^2 \delta(K) + k^2 \Omega \Psi(K) \right] d^2r \quad (A17)$$

where  $\Omega$  depends only on the geometry and elastic constants of both media,

$$\Psi(K) = \frac{1}{(2\pi)^2} \int \langle \zeta(x) \zeta(x+y) \rangle e^{iK \cdot y} d^2y \quad (A18)$$

$$\Omega = \left[ \frac{R'}{R_0} + \frac{\gamma'}{\gamma_0} \right]^2 + (\alpha T')^2, \quad (A19)$$

where the prime means derivative with respect to  $\zeta$ , and subscript 0 refers to  $\zeta = 0$ .

The first term of the right hand side of (A17) contributes to the specular direction, because  $K = 0$  is just Snell's law. The second term describes finite angle scattering waves and has a similar form to that for the volumetric inhomogeneities obtained in (A9), except for the geometry factor  $\Omega$ . The validity of this method is limited to topographic irregularities with radius of curvature larger than the wavelength, so that locally plane reflection/transmission coefficients can be used, or  $h \ll L$  and  $\lambda \ll L^2/8h$ , where  $h$  and  $L$  are the characteristic height and length of the irregularity respectively, and  $\lambda$  is the seismic wavelength. In the application of this method to  $PKP$  waves where scattering occurs at the CMB, the wavelength of  $P$  waves of 1 Hz is typically about 13 km, so that this method can be used for irregularities with heights of up to 1 km and wavelengths not smaller than 10 km.

**Acknowledgments.** The authors are grateful to R.S. Wu for discussions. Partial funding for this research has been provided by Defense Advanced Research Projects Agency grant MDA903-86-K-0010 and by the W. M. Keck Foundation.

### REFERENCES

Ahrens, T. J., and B. H. Hager, Heat transport across D": problems and paradoxes, *Trans. AGU*, 68, 1493, 1987.

- Alexander, S. S., and R. A. Phinney, A study of the core-mantle boundary using *P* waves diffracted by the earth's core, *J. Geophys. Res.*, **71**, 5943-5958, 1966.
- Bataille, K., Inhomogeneities near the core-mantle boundary inferred from short-period scattered waves recorded at GDSN, Ph.d. thesis, Univ. of Calif. Santa Cruz, 1987.
- Boss, A. P., and I. S. Sacks, Formation and growth of deep mantle plumes, *Geophys. J. R. Astron. Soc.*, **80**, 241-255, 1985.
- Chernov, L. A., *Wave Propagation in a Random Medium*, Mc Graw-Hill, New York, 1960.
- Cornier, V. F., Some problems with *S*, *SKS*, and *ScS* observations and implications for the structure of the base of the mantle and the outer core, *J. Geophys.*, **57**, 14-22, 1986.
- Creager, K. C., and T. H. Jordan, Aspherical structure of the core-mantle boundary from PKP travel times, *Geophys. Res. Lett.*, **13**, 1497-1500, 1986.
- Doombos, D. J., Characteristics of lower mantle inhomogeneities from scattered waves, *Geophys. J. R. Astron. Soc.*, **44**, 447, 1976.
- Doombos, D. J., On seismic-wave scattering by a rough core-mantle boundary, *Geophys. J. R. Astron. Soc.*, **53**, 643-662, 1978.
- Doombos, D. J., and J. C. Mondt, *P* and *S* waves diffracted around the core and the velocity structure at the base of the mantle, *Geophys. J. R. Astron. Soc.*, **57**, 353-379, 1979.
- Doombos, D. J., S. Spiliopoulos, and F. D. Stacey, Seismological properties of D" and the structure of a thermal boundary layer, *Phys. Earth Planet. Inter.*, **41**, 225-239, 1986.
- Dziewonski, A. M., and D. L. Anderson, Preliminary reference earth model, *Phys. Earth Planet. Inter.*, **25**, 297-356, 1981.
- Flatté, S. M., and R. S. Wu, Small-scale structure in the lithosphere and asthenosphere deduced from arrival-time and amplitude fluctuations at NORSAR, *J. Geophys. Res.*, **93**, 6601-6614, 1988.
- Frazer, L. N., and M. K. Sen, Kirchhoff-Helmholtz reflection seismograms in a laterally inhomogeneous multilayered elastic medium: I. Theory, *Geophys. J. R. Astron. Soc.*, **80**, 121-147, 1985.
- Haddon, R. A. W., and J. R. Cleary, Evidence for scattering of seismic PKP waves near the core-mantle boundary, *Phys. Earth Planet. Inter.*, **8**, 211, 1974.
- Husebye, E. S., D. W. King, and R. A. W. Haddon, Precursors to PKIP and seismic wave scattering near the core-mantle boundary, *J. Geophys. Res.*, **81**, 1870, 1976.
- Jones, G. M., Thermal interaction of the core and mantle and long term behavior of the geomagnetic field, *J. Geophys. Res.*, **82**, 1703-1709, 1977.
- Jeanloz, R., and F. M. Richter, Convection, composition and thermal state of the lower mantle, *J. Geophys. Res.*, **84**, 5497-5504, 1979.
- Jordan, T. H., and K. C. Creager, Chemical boundary layers of the mantle and core, *Trans. AGU*, **68**, 1494, 1987.
- Kennett, B. L. N., Seismic wave scattering by obstacles on interfaces, *Geophys. J. R. Astron. Soc.*, **28**, 249-266, 1972.
- King, D. W., R. A. W. Haddon, J. Cleary, Array analysis of precursors to PKIP in the distance range 128° to 143°, *Geophys. J. R. Astron. Soc.*, **37**, 157-173, 1974.
- Knittle, E., and R. Jeanloz, High-Pressure metallization of FeO and implications for the earth's core, *Geophys. Res. Lett.*, **13**, 1541-1544, 1986.
- Knittle, E., Q. Williams, and R. Jeanloz, Reaction of core constituents with silicates and oxides: implications for the composition of the core-mantle boundary, *Trans. AGU*, **68**, 1210, 1987.
- Knopoff, L., and J. A. Hudson, Scattering of elastic waves by small inhomogeneities, *J. Acoust. Soc. Am.*, **36**, 338-343, 1964.
- Lay, T., and D. V. Helmberger, A shear velocity discontinuity in the lower mantle, *Geophys. Res. Lett.*, **10**, 63-66, 1983.
- Loper, D. E., and K. McCartney, Mantle plumes and the periodicity of magnetic field reversals, *Geophys. Res. Lett.*, **13**, 1525, 1986.
- Menke W., Few 2-50 km corrugations on the core-mantle boundary, *Geophys. Res. Lett.*, **13**, 1501-1504, 1986.
- Mitchell, B. J., and D. V. Helmberger, Shear velocities at the base of the mantle from observations of *S* and *ScS*, *J. Geophys. Res.*, **78**, 6009-6020, 1973.
- Morelli, A., and A. M. Dziewonski, Topography of the core-mantle boundary and lateral homogeneity of the liquid core, *Nature*, **325**, 678-683, 1987.
- Mula, A. H. and G. Muller, Ray parameters of diffracted long-period *P* and *S* waves and the velocities at the base of the mantle, *Pure Appl. Geophys.*, **118**, 1272-1292, 1980.
- Olson, P., G. Schubert, and C. Anderson, Plume formation in the D"-layer and the roughness of the core-mantle boundary, *Nature*, **327**, 409-413, 1987a.
- Olson, P., G. Schubert, and C. Anderson, Boundary layer dynamics and small-scale structure at the base of the mantle, *Trans. AGU*, **68**, 1488, 1987b.
- Poupinet, G., R. Pilet, and A. Souriau, Possible heterogeneity of the earth's core deduced from PKIP travel time, *Nature*, **305**, 204-206, 1983.
- Ringwood, A. E., *Composition and Petrology of the Earth's Mantle*, McGraw-Hill, New York, 1979.
- Ritzwoller, M., G. Masters, and F. Gilbert, Observations of anomalous splitting and their interpretation in terms of aspherical structure, *J. Geophys. Res.*, **91**, 10203-10228, 1986.
- Schlittenhardt, J., J. Schweitzer, and G. Muller, Evidence against a discontinuity at the top of D", *Geophys. J. R. Astron. Soc.*, **81**, 295-306, 1985.
- Sen, M. K., and N. L. Frazer, Kirchhoff-Helmholtz reflection seismograms in a laterally inhomogeneous multi-layered elastic medium: II. Computations, *Geophys. J. R. Astron. Soc.*, **82**, 415-437, 1985.
- Scott, P. F., and D. V. Helmberger, Applications of the Kirchhoff-Helmholtz integral to problems in seismology, *Geophys. J. R. Astron. Soc.*, **72**, 237-254, 1983.
- Stacey, F. D., and D. E. Loper, The thermal layer interpretation of D" and its role as a plume source, *Phys. Earth Planet. Inter.*, **33**, 45-55, 1983.
- Van der Berg, A. P., S. A. P. L. Cloetingh, and D. J. Dobos, A comparison of PKP precursor data from several seismic arrays, *J. Geophys.*, **44**, 499-510, 1980.
- Wu, R. S., and K. Aki, Scattering characteristics of elastic waves by an elastic heterogeneity, *Geophysics*, **50**, 582-595, 1985a.
- Wu, R. S., and K. Aki, Elastic wave scattering by a random medium and the small-scale inhomogeneities in the lithosphere, *J. Geophys. Res.*, **90**, 10,261-10,273, 1985b.
- Yuen, D. A., and W. R. Peltier, Mantle plumes and the thermal stability of the D" layer, *Geophys. Res. Lett.*, **7**, 625-628, 1980.

K. Bataille and S.M. Flatté, Physics Department and Institute of Tectonics, University of California at Santa Cruz, Santa Cruz, CA 95064.

(Received February 19, 1988;  
revised June 29, 1988;  
accepted June 9, 1988.)

# Small-Scale Structure in the Lithosphere and Asthenosphere Deduced From Arrival Time and Amplitude Fluctuations at NORSAR

STANLEY M. FLATTÉ AND RU-SHAN WU

*Physics Department and Institute of Tectonics, University of California, Santa Cruz*

We analyze the pattern of phase and amplitude variations of seismic waves across the NORSAR array on a statistical basis in order to determine the statistical distribution of heterogeneities under NORSAR. Important observables that have been analyzed in the past are the phase (or travel time) and log amplitude variances and the transverse coherence functions (TCFs) of phase and amplitude fluctuations. We propose and develop the theory and methods of using other observables to reduce the degree of nonuniqueness and increase the spatial resolution of the analysis. Most important are the angular coherence functions (ACFs), which characterize quantitatively the change in the pattern of fluctuations across the array from one incoming angle (or beam) to another and which have a different sensitivity to the depth distribution of heterogeneities than the TCFs. A combination of the ACFs and TCFs allows estimation of the power spectra of the  $P$  wave speed variations under the array as a function of depth. We use data for phase fluctuations from 104 incident beams and amplitude fluctuations from 185 beams with 2-Hz center frequency at NORSAR to calculate the three ACFs and three TCFs (of phase, log amplitude, and their cross coherence). The measured rms travel time fluctuation is 0.135 s, and the rms log amplitude fluctuation is 0.41. The half-coherence widths of the ACFs are  $3^\circ$  for log amplitude and  $9^\circ$  for phase. The half-coherence widths of the TCFs are 18 km for phase and less than the minimum separation between the elements of the array for log amplitude. In order to account for these features of the data, we adopt a two-overlapping-layer model for lithospheric and asthenospheric heterogeneities underneath NORSAR, with spectra that are band-limited between the wavelengths of 5.5 and 110 km. Our best model has an upper layer with a flat power spectrum extending from the surface to about 200 km, and a lower layer with a  $K^{-4}$  power spectrum extending from 15 to 250 km. The latter spectrum corresponds to an exponential correlation function with scale larger than the observation aperture (110 km). The rms  $P$  wave speed variations lie in the range 1–4%. The small scale heterogeneities may be attributed to clustered cracks or intrusions; the larger-scale wave-speed heterogeneities are temperature or compositional heterogeneities that may be related to chemical differentiation, or dynamical processes in the boundary layer of mantle convection.

## 1. INTRODUCTION

Observations of direct  $P$  wave amplitude and arrival time fluctuations [Aki, 1973; Capon, 1974; Capon and Berteussen, 1974; Berteussen et al., 1975a, b; Powell and Meltzer, 1984], coda strength [Aki, 1981; Sato, 1982; Wu and Aki, 1985a, b], and attenuation by scattering [Aki and Chouet, 1975; Aki, 1980; Wu, 1982; Sato, 1982] have all been used in attempts to determine some statistical characteristics of small-scale structure in the Earth. Statistical analyses of amplitude and arrival time fluctuations have previously involved the variances of log amplitude and arrival time, the covariance of log amplitude and arrival time, and the coherence functions of log amplitude and arrival time as functions of spatial separation along the Earth's surface (the transverse coherence functions, or TCFs) [Aki, 1973; Capon, 1974; Capon and Berteussen, 1974; Berteussen et al., 1975a, b; Powell and Meltzer, 1984].

Theoretical analyses of the observations assume a particular medium structure and, by various techniques, compare theoretical predictions of seismic wave properties to the observations. Previous seismic wave analyses followed Chernov [1960], who used the Rytov and Fresnel approximations to connect wave fluctuations to medium variations. His expressions involving general random media in the space domain are formidable, but he evaluated them explicitly for a statistically uniform and iso-

tropic random medium with a Gaussian correlation function; his resulting expressions have been used by previous workers to obtain strengths and scale sizes of the  $P$  wave speed variations in the lithosphere by modeling it as a uniform layer of a single-scale random medium.

This paper has several purposes: first, to point out that the log amplitude and arrival time fluctuations at large seismic arrays like NORSAR and LASA have further important statistical information that has not been utilized in previous analyses, especially the coherence function of waves from different sources, and hence different incoming directions; second, to present a statistical analysis of NORSAR data that includes this new information; third, to present results from the modern theory of wave propagation through random media (WPRM) that are based on the parabolic wave equation approach and are somewhat simpler than Chernov's because they are formulated partially in the spectral domain and can accommodate easily any model of the medium spectrum; and fourth, to present a model of the inhomogeneities in the lithosphere and asthenosphere under the NORSAR array that is consistent with the available data.

Before discussing the most interesting of the new information available, it is important to point out that there are three variances involved in arrival time and log amplitude fluctuations at a given seismic frequency; the variances of arrival time and log amplitude, and the covariance between the two. Each of these variances leads to a coherence function of any variable being investigated; for example, previous analyses [Aki, 1973; Capon, 1974; Capon and Berteussen, 1974; Berteussen et al., 1975a, b;

Copyright 1988 by the American Geophysical Union.

Paper number 7B5081.  
0148-0227/88/007B-5081\$05.00

The U.S. Government is authorized to reproduce and sell this report. Permission for further reproduction by others must be obtained from the copyright owner. 6601



Powell and Meltzer, 1984] have used the arrival time and log amplitude transverse coherence functions, but we will be analyzing here for the first time the transverse cross-coherence function between arrival time and log amplitude.

The main new information that can be obtained from an array that detects waves arriving from many directions ("beams") is the set of three angular coherence functions (ACFs): that is, the coherence functions of arrival time, log amplitude, and their cross coherence, all as a function of the angle between two incoming directions. Since the difference in direction between two beams may be as small as  $1^\circ$ , the information at a given receiver probes (in a statistical sense) inhomogeneities that are quite small: of the order of 1 km at 60-km depth. The transverse coherence functions from a coarse array with ~10-km spacing cannot probe to scales smaller than 10 km.

Data on arrival time and amplitude fluctuations of the first-arrival teleseismic *P* wave signal are analyzed in a different fashion than data involving large-angle scattering of wave energy. The difference involves the realization that the full wave equation need not be solved, but rather a simpler equation: the parabolic wave equation (PWE) that adequately treats waves in a narrow angular cone. (Note that if coda is interpreted as large-angle scattered waves, it cannot be treated in the same way.) One consequence of using the PWE is that the theoretical formulas are easily expressed in terms of an integral along the unperturbed ray, rather than as a volume integral over all of space. Section 2 briefly introduces the modern theory of WPRM theory based on the PWE and "weak" fluctuations. Section 3 specifically describes the theory of the angular coherence functions.

The NORSAR data used in our analysis consist of the travel time anomalies [Berteussen, 1974] at 22 subarrays for 104 beams; and the log amplitude fluctuations [Berteussen and Husebye, 1974] at 22 subarrays for 185 beams. All the beams have incoming directions within a  $35^\circ$  cone around the zenith. The smallest distance between subarrays is about 10 km, and the largest is about 110 km. The data used were filtered for 1–3 Hz, so the nominal frequency is 2 Hz. It is important to realize that the data that we analyze are insensitive to inhomogeneities with wavelengths greater than about 100 km because of the finite size of the array and are also insensitive to inhomogeneity wavelengths less than about 5 km because of two effects: first the data are averages over subarrays that are 7 km in diameter, and second, the wavelengths of the seismic waves are about 4 km. Section 4 describes the data analysis and presents results for coherence functions at NORSAR.

It does not take a sophisticated theory to draw some dramatic conclusions from this new analysis of NORSAR data. Briefly, the log amplitude ACF drops rapidly, reaching a value of 0.5 at an angle of  $2^\circ$ , followed by a more gradual drop to 0.1 at  $10^\circ$ . In contrast, the arrival-time ACF drops much more slowly, implying much larger-scale structure. Yet all the TCFs at first glance have scales in the range of 10–20 km. Section 5 contains the quantitative comparison of weak scattering models with the NORSAR data. We have found that medium spectral models that are homogeneous in depth (that is, the spectrum does not change with depth) down to a cutoff depth between 0 and 500 km cannot fit all the data at once; in particular, such models, which can fit the TCFs by themselves, cannot simultaneously fit the shapes of the ACFs. We suggest a two-overlapping-layer model in which the medium spectrum is characterized by a power law  $K^{-p}$  over the sensitive wave number band

( $5 < \lambda < 100$  km). An upper layer with significant small-scale structure ( $p = 0$ ) spans  $0 < z < 200$  km and a lower layer with strength concentrated at large scales ( $p = 4$ ) spans  $15 < z < 250$  km. The *P* wave rms velocity variations in our model vary between 1 and 4%. A specific prediction of the model that we suggest is a rapid drop in the log amplitude TCF for separations of a few kilometers, followed by a more gradual drop with a scale of tens of kilometers. We have checked this prediction by determining the TCF of log amplitude from the individual stations at NORSAR, using 13 nuclear explosion events. We find consistency with our prediction, giving us some confidence in our interpretation.

## 2. THEORY OF WPRM

Many aspects of seismic wave propagation in the Earth involve examples of a more general branch of science; namely, wave propagation through random media (WPRM). Progress in this field has involved coupling of the theory of WPRM with investigation into the detailed character of the (generally fluid) random medium. At least two theoretical approaches may be taken: first, the problem may be approached from a deterministic point of view in which the analysis is carried out for particular complex media. Numerical simulation is the extreme of this point of view. Second, the problem may be treated statistically from the outset. In this approach, one assumes a spectral model for the medium and attempts by analytical means to predict the statistical behavior of the propagating wave field. Here we take this second point of view.

The modern theory of WPRM may be said to have begun in the late 1940s and early 1950s [Bergmann, 1946; Mintzer, 1953; Chernov, 1960; Tatarskii, 1971] when researchers used perturbation techniques to develop general formulas for propagation through weak fluctuations. These formulas involved the Born approximation and hence a volume integral over the medium inhomogeneities. In comparing with experiment they assumed that the medium was characterized by a Gaussian correlation function, but unfortunately, no natural medium is known with this property.

The problem of radio wave propagation in and through the Earth's ionosphere has been of interest since the 1940s. This field made a crucial contribution to WPRM through the work of Leontovich and Fock [1946] and Fock [1950], who introduced the parabolic equation method, which treats waves that are concentrated within a small angular region around the direction of propagation. Nearly all subsequent analytic work has used the parabolic equation as a starting point, which restricts validity to waves with directions confined within a cone of full angle about  $30^\circ$ . A great advantage of the parabolic equation is that it results in formulas requiring line integrals along deterministic rays, rather than volume integrals.

A major step forward in WPRM was taken in the 1960s, in response to developing understanding of Kolmogorov's pioneering characterization of the  $p = 11/3$  power law spectrum of homogeneous, isotropic turbulence (HIT). A theory for wave propagation through HIT was developed, primarily by Soviet workers, and successfully applied in the case of weak fluctuations to light transmission through the atmosphere, making use of the parabolic equation. Their work was summarized in the influential book by Tatarskii [1971] and a review article by Prokhorov et al. [1975], and more recent results in this field are covered in the review articles by Ishimaru [1977], Fante [1980],

and Tatarskii and Zavorotnyi [1980], as well as in the book edited by Strohbehn [1978].

It is now understood that weak fluctuation theory applies when the variance of log amplitude is small compared with unity. We realize that many seismic data sets have large intensity variations, but in this paper we consider only those for which the log amplitude variance is small. For example, the NORSAR data set of subarray amplitude variations has a log amplitude variance of 0.2. We defer discussion of the problem of strong fluctuations to the future.

Seismic rays often turn through large angles, so that the parabolic approximation is not clearly appropriate. However, if the wave fluctuations are caused by medium variations that are confined to regions near the source and receiver (within a few hundred kilometers), then the rays are not changing their angles significantly, and the parabolic approximation is valid.

Work on fluctuations in sound transmission through the ocean during the 1960s was largely a misguided attempt to graft the concept of HIT onto ocean variability [Tatarskii, 1971]. By the mid-1970s, oceanographers had identified internal waves as the most important source of variability on time scales from a few minutes to a day [Garrett and Munk, 1975].

The ocean internal wave medium provided a challenge to those interested in WPRM, particularly in strong fluctuations. A significant response to this challenge was developed over the late 1970s. The first success in this area was achieved for weak fluctuations by Munk and Zachariasen [1976], whose absolute calculations of variances in phase and log amplitude from internal wave effects were within a factor of 2 of the available experimental results. Strong fluctuations were another matter.

A further basic step forward took place between 1975 and 1977, with the consideration of the arbitrary field of wave speed in Feynman's path integral as a statistical random medium [Dashen, 1979; Flatté et al., 1979], in combination with the understanding of the ocean internal wave field as the source of medium fluctuations. These ideas led to successful comparisons with a number of ocean acoustics experiments, summarized in the monograph by Flatté et al. [1979], the review article by Flatté [1983], and subsequent publications [Dashen et al., 1985; Reynolds et al., 1985; Flatté and Stoughton, 1986; Stoughton et al., 1986; Flatté et al., 1987a, b].

With this background in mind, we now apply parabolic equation, weak-scattering theory to  $P$  wave teleseismic propagation. We take the point of view that the seismic waves arrive a few hundred kilometers below an array like NORSAR in essentially plane wave form: that any effect due to inhomogeneities near the source is too large scale to be observed by a 100-km array and that the very deep mantle has imposed no significant structure on the wave that has scales less than the 100-km size of the array. The reason that the inhomogeneities near the source have little effect is that only a very small range of initial angles at the source is seen by the array, and the spreading of the ray tube magnifies any small-scale fluctuations of the wave front into large-scale fluctuations at the receiver.

Furthermore we assume that the effect on the arrival time and amplitude fluctuations of inhomogeneities within a few hundred kilometers depth below the array results mainly from wave scattering within a reasonably narrow cone. We realize that coda can represent scattering at larger angles; however, the first few seconds of  $P$  wave arrivals are restricted to small angles.

Since NORSAR data (by subarray) show a log amplitude variance of 0.2, we use weak fluctuation theory. It has been

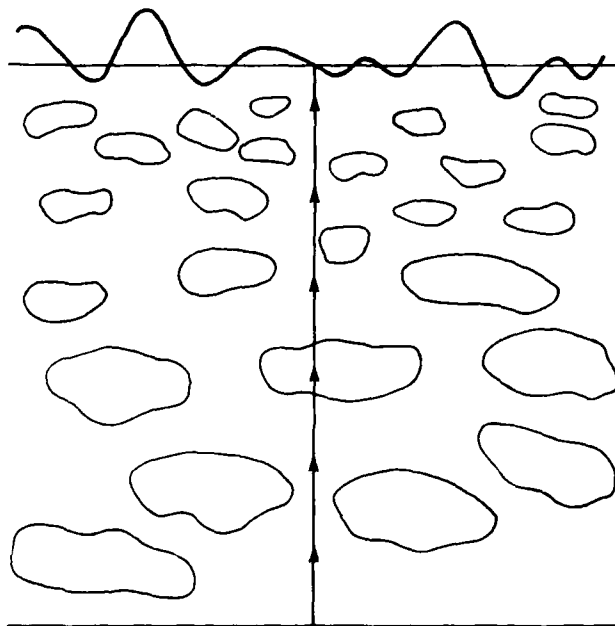


Fig. 1. Schematic of  $P$  wave propagation through the upper mantle, lithosphere, and crust to a surface seismic array. The heavy solid straight line is the incident wave front, the light solid horizontal line is the wave front arriving at the receiving array in the absence of fluctuations. The wavy line could represent either the wave front arrival time across the array or the intensity at each point in the arriving wave front.

established that even if intensity fluctuations are large, if they are averaged over a small source (or receiver) region, such that the residual (larger scale) intensity fluctuations are small, then weak-fluctuation theory can be applied [Wang et al., 1978]. There are probably aspects of this averaging in the NORSAR data because of the 7-km width of a typical subarray and because of finite wavelength effects, which result in the observed log amplitude variance of 0.2.

Finally, we neglect the small deterministic refraction in the few hundred kilometers below the array; in the absence of inhomogeneities, the wave fronts remain plane in the same direction. (See Figure 1.)

We now state the results of weak-scattering theory under the above restrictions. First, define the medium  $P$  wave speed as a function of position:

$$C(\underline{x}) = C_0 [1 + \mu(\underline{x})] \quad (1)$$

where  $C_0$  is a reference deterministic speed that might depend on depth  $z$ , and  $\mu(\underline{x})$  is a random function with zero mean that represents inhomogeneities. The statistics of  $\mu$  are assumed to be quasi-homogeneous. That is, we can define a spectrum at depth  $z$ , and this spectrum is allowed to change slowly with depth. In this case, the character of  $\mu(\underline{x})$  is described by a three-dimensional spectrum  $W(\underline{K}, z)$ , such that

$$\langle \mu(\underline{x}) \mu(\underline{x}') \rangle = \int d^3 \underline{K} W(\underline{K}, z) e^{i \underline{K} \cdot (\underline{x} - \underline{x}')} \quad (2)$$

where we have assumed that the spectrum depends on a three-dimensional wave vector  $\underline{K}$  and depth  $z$ , and the angle brackets represent an average over the statistical ensemble of random media. Since the spectrum does not depend on transverse posi-

tion and depends only slowly on depth  $z$ , the medium correlation function  $\langle \mu(\underline{x})\mu(\underline{x}') \rangle$  depends only on the difference vector  $\underline{x} - \underline{x}'$ , except for a slow dependence on  $z$  which is implicit. Note the normalization of the spectrum is such that

$$\langle \mu^2 \rangle = \int d^3 \underline{K} W(\underline{K}, z) \quad (3)$$

where  $\langle \mu^2 \rangle$  is the variance of the fractional change in wave speed due to the random inhomogeneities; it can depend on depth  $z$ .

Consider a given frequency  $\omega$  in the incoming wave. That frequency has wave number  $k = \omega/C_0$ . Let the complex wave function arriving at the center of the array be

$$\Psi = Ae^{i\phi}\Psi_0 \quad (4)$$

where  $\Psi_0$  is the wave function that would arrive in the absence of the random inhomogeneities and where the amplitude  $A$  and phase  $\phi$  are defined in this relation. Define the log amplitude as  $u$ , so that

$$\ln(\Psi/\Psi_0) = u + i\phi \quad (5)$$

It is known in the case of weak scattering confined to an narrow cone, in an intrinsically dispersion-free medium, that the arrival time fluctuation  $\tau$  and the phase fluctuation  $\phi$  are in one-to-one correspondence:

$$\phi = \omega\tau$$

We now point out that for a specific realization of inhomogeneities,  $u$  and  $\phi$  are functions of both the receiver position  $\underline{x}$  and the source position, represented by a unit vector  $\underline{\theta}$  describing the direction of the incoming plane wave. (See Figure 1.)

Note first that we have made the approximation that the random medium is "horizontally homogeneous"; that is, the spectrum is independent of horizontal position. We also consider waves arriving within  $30^\circ$  of the zenith, so we avoid some simple geometrical corrections that are important only for highly slanted rays. We can split the three-dimensional wave number

$\underline{K}$  into a component along the  $z$  direction  $K_z$  and a two-dimensional vector  $\underline{K}_T$  transverse to  $z$ ; that is,  $\underline{K}_T$  is in the  $x$ - $y$  plane. Then the medium spectrum can be expressed as

$$W(\underline{K}, z) = W(K_z, \underline{K}_T, z) \quad (6)$$

With the above definitions and approximations, the result [Munk and Zachariasen, 1976; Flatté et al., 1979; S.M. Flatté and T. Moody, manuscript in preparation, 1987] for the variances of the seismic wave fluctuations at the surface of the earth are

$$\langle u^2 \rangle = 2\pi k^2 \int_0^R dz \int d^2 \underline{K}_T W(0, \underline{K}_T, z) \sin^2(K_T^2 z/2k) \quad (7)$$

$$\langle \phi^2 \rangle = 2\pi k^2 \int_0^R dz \int d^2 \underline{K}_T W(0, \underline{K}_T, z) \cos^2(K_T^2 z/2k) \quad (8)$$

$$\langle u\phi \rangle = 2\pi k^2 \int_0^R dz \int d^2 \underline{K}_T W(0, \underline{K}_T, z) \sin[K_T^2 z/2k] \cos[K_T^2 z/2k] \quad (9)$$

where  $R$  is the depth of the deepest inhomogeneities being analyzed.

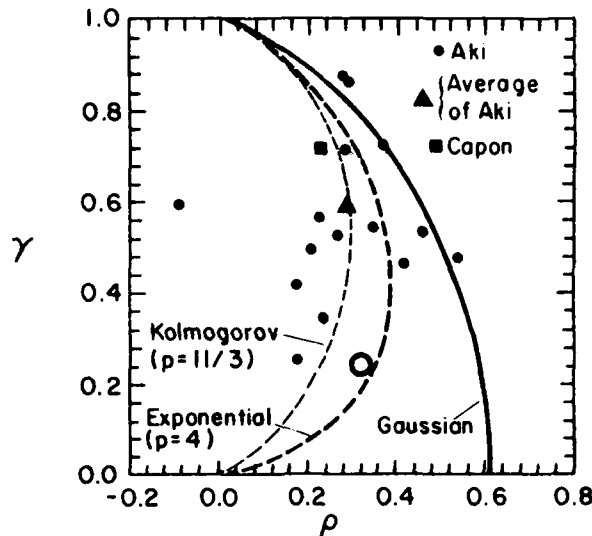


Fig. 2. Variance ratio  $\gamma$  versus amplitude-phase correlation  $\rho$  for uniform extended media. The solid circles are from Aki [1973]. The solid squares are from Capon [1974]. The open circle comes from our analysis of NORSAR data. The quantity  $p$  is the spectral power law index (equation (30)). Position along one of the curves is determined by the wave parameter  $D = 4R/ka^2$  where  $R$  is the propagation range,  $k$  is the wave number, and  $a$  is the correlation length.

An example of information to be gained from evaluation of the variances is given in Figure 2, which plots the two quantities

$$\gamma = \frac{u_{\text{rms}}}{\phi_{\text{rms}}} \quad (10)$$

$$\rho = \frac{\langle u\phi \rangle}{u_{\text{rms}} \phi_{\text{rms}}} \quad (11)$$

where  $u_{\text{rms}}^2 = \langle u^2 \rangle$  and  $\phi_{\text{rms}}^2 = \langle \phi^2 \rangle$ . Both  $\gamma$  and  $\rho$  are ratios that do not depend on the overall strength  $\langle \mu^2 \rangle$  of the inhomogeneities. For a medium that extends to depth  $R$  with fluctuation statistics that are independent of depth, both  $\gamma$  and  $\rho$  depend on one parameter. Given a scale  $a$  that characterizes the spectrum  $W(\underline{K})$ , that parameter is  $D = 4R/(ka^2)$ , which was defined as the wave parameter by Chernov [1960]. For each choice of medium spectrum there is a unique curve in  $\gamma$ - $\rho$  space traced out through different values of  $D$ . Some examples are given in Figure 2 along with some experimental results. It is seen that spectra of the power law type are a better fit to the variances than a Gaussian spectrum and that the values of  $\rho$  cluster around 0.3, while the values of  $\gamma$  vary substantially. Note that higher seismic frequencies will tend to have lower  $\gamma$  because  $\phi_{\text{rms}}$  increases with frequency faster than  $u_{\text{rms}}$ . Of course, a medium whose spectrum is dependent in some way on depth will lead to  $p$ ,  $\gamma$  values that do not lie on these sample curves, but the general trend of smaller  $\rho$  for power law spectra versus Gaussian spectra will apply.

Further information beyond the variances is available in coherence functions. For example, the phase coherence between two receivers at positions  $\underline{x}_{1T}$  and  $\underline{x}_{2T}$  can be expressed as

$$\langle \phi(\underline{x}_{1T})\phi(\underline{x}_{2T}) \rangle = \langle \phi(\underline{x}_T)\phi(0) \rangle \quad (12)$$

where we have defined  $\underline{x}_T = \underline{x}_{2T} - \underline{x}_{1T}$  and we have used horizontal homogeneity of the spectrum. We define the transverse

coherence functions (TCFs) corresponding to each of the above variances  $\langle u(x_T) u(0) \rangle$ ,  $\langle \phi(x_T) \phi(0) \rangle$ , and  $\langle u(x_T) \phi(0) \rangle$ , respectively. Again, since horizontal homogeneity of the spectrum is assumed, these functions depend only on the difference between the two positions. The expression for the TCFs in terms of the medium spectrum are (Flatté and Moody, manuscript in preparation, 1987)

$$\langle u(x_T) u(0) \rangle = 2\pi k^2 \int_0^R dz \int d^2 K_T W(0, K_T, z) \sin^2[K_T^2 z/2k] \cos[K_T \cdot x_T] \quad (13)$$

$$\langle \phi(x_T) \phi(0) \rangle = 2\pi k^2 \int_0^R dz \int d^2 K_T W(0, K_T, z) \cos^2[K_T^2 z/2k] \cos[K_T \cdot x_T] \quad (14)$$

$$\langle u(x_T) \phi(0) \rangle = 2\pi k^2 \int_0^R dz \int d^2 K_T W(0, K_T, z) \cos[K_T^2 z/2k] \sin[K_T^2 z/2k] \cos[K_T \cdot x_T] \quad (15)$$

Since  $W$  is assumed not to depend on the direction of  $K_T$  but only its magnitude (horizontal isotropy), the  $K_T$  integral can be expressed in polar coordinates, and the angular integral may be done. The results are then a function only of the magnitude of the separation  $x_T$  and not its direction:

$$\langle u(x_T) u(0) \rangle = 4\pi^2 k^2 \int_0^R dz \int_0^\infty K_T dK_T W(0, K_T, z) \sin^2[K_T^2 z/2k] J_0(K_T x_T) \quad (16)$$

$$\langle \phi(x_T) \phi(0) \rangle = 4\pi^2 k^2 \int_0^R dz \int_0^\infty K_T dK_T W(0, K_T, z) \cos^2[K_T^2 z/2k] J_0(K_T x_T) \quad (17)$$

$$\langle u(x_T) \phi(0) \rangle = 4\pi^2 k^2 \int_0^R dz \int_0^\infty K_T dK_T W(0, K_T, z) \sin[K_T^2 z/2k] \cos[K_T^2 z/2k] J_0(K_T x_T) \quad (18)$$

We find it convenient to work with normalized TCFs defined as follows:

$$\langle \phi(x_T) \phi(0) \rangle_N = \frac{\langle \phi(x_T) \phi(0) \rangle}{\langle \phi^2 \rangle} \quad (19)$$

$$\langle u(x_T) u(0) \rangle_N = \frac{\langle u(x_T) u(0) \rangle}{\langle u^2 \rangle} \quad (20)$$

$$\langle u(x_T) \phi(0) \rangle_N = \frac{\langle u(x_T) u(0) \rangle}{u_{\text{rms}} \phi_{\text{rms}}} \quad (21)$$

These normalized functions, like the quantities  $\gamma$  and  $\rho$ , do not depend on the overall strength  $\langle \mu^2 \rangle$  of the medium fluctuations. We note that the values of these coherences at  $x_T = 0$  are 1, 1, and  $\rho$ , respectively.

Note that our expressions for the variances and the TCFs are simpler than the usual Born approximation volume-integration expressions (S.M. Flatté and T. Moody, manuscript in preparation, 1987). Here we have a one-dimensional integral along  $z$  and a one-dimensional integral over the spectrum. We see that

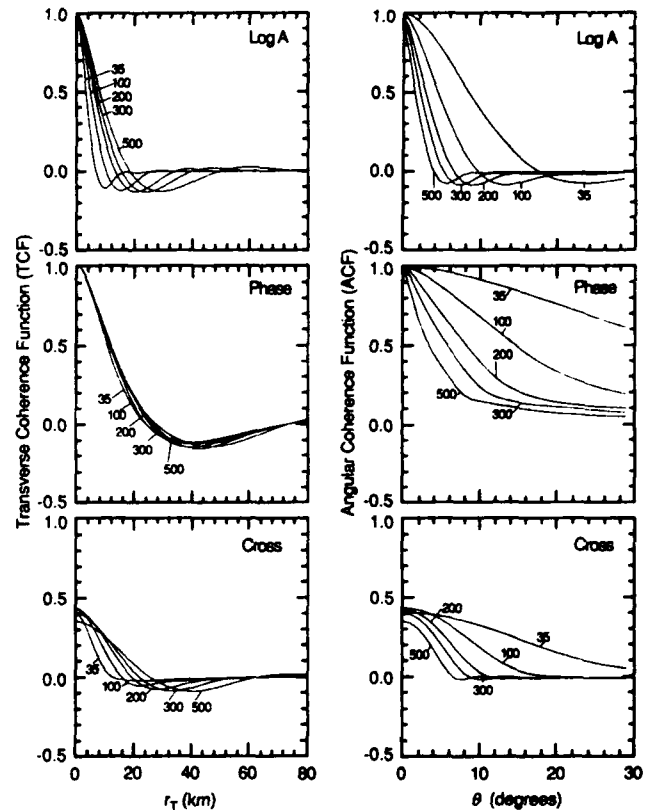


Fig. 3. The three transverse coherence functions (TCFs) and the three angular coherence functions (ACFs) for an extended medium with an exponential correlation function with scale  $a = 10$  km and a seismic frequency of 1 Hz. The different curves are results for media that extend from the surface to different depths given by the curve labels in kilometers: that is, varying from 35 to 500 km.

the log amplitude fluctuation  $u$  is weighted toward higher wave number  $K_T$  than the phase fluctuation due to the "Fresnel filter" factors  $\sin^2[K_T^2 z/2k]$  and  $\cos^2[K_T^2 z/2k]$ . We also see that this weighting is more pronounced for smaller  $z$ ; in other words, fluctuations of  $u$  with wavelengths  $\lambda_K > 2\pi(z/k)^{1/2}$  are suppressed. Note that there is more suppression near the surface; it is difficult for wave speed fluctuations to cause amplitude fluctuations without a sufficient drift space before the receiver.

It is helpful to show some examples of the normalized TCFs for an interesting medium spectrum. Figure 3 shows the three TCFs for a medium with an exponential correlation function with scale  $a = 10$  km. That is,

$$W(K) = \frac{\langle \mu^2 \rangle a^3}{\pi^2} \frac{1}{(1 + K^2 a^2)^2} \quad (22)$$

We see that the width of the phase coherence function is larger than the width of the medium correlation function, while the width of the log amplitude coherence function is smaller. This is due to the Fresnel-filter factor which favors high wave number and hence small scales in the log amplitude coherence.

### 3. ANGULAR CORRELATION FUNCTIONS

Consider teleseismic waves arriving from two different directions indicated by unit vectors  $\theta_1$  and  $\theta_2$ ; let the vectorial

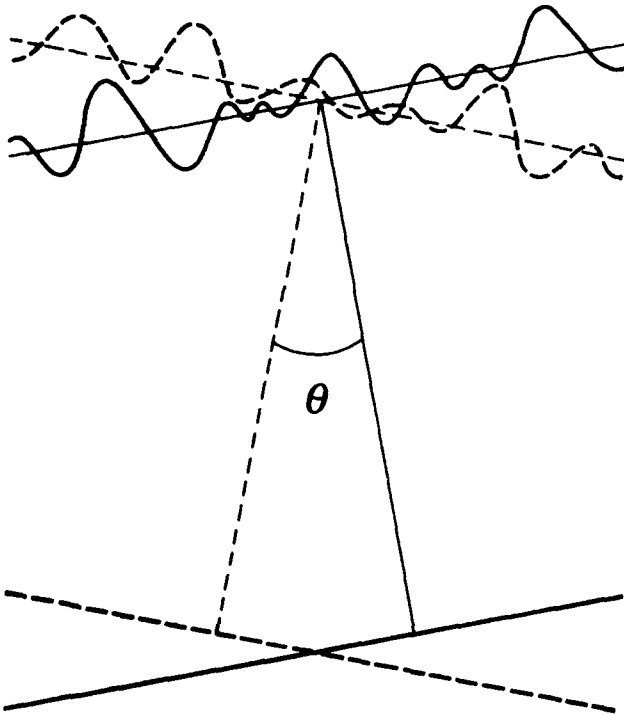


Fig. 4. Schematic of incident  $P$  waves from two different sources incident on a seismic array (see Figure 1).

difference in angle be  $\theta = \theta_2 - \theta_1$ . Finally, the magnitude of the angle between the two unit vectors is denoted by  $\theta$ . It is well known that the patterns of  $u$  and  $\phi$  on the Earth's surface will be different for waves from the two different directions, and this difference will be greater for larger angular differences: that is, larger  $\theta$ . (See Figure 4.) If we again make the assumption of horizontal homogeneity and isotropy of the medium fluctuation spectrum, then statistical correlation between the log amplitudes and phases of the waves from two different directions will be a function only of the magnitude of the angular difference between the two waves; that is, the magnitude of  $\theta$  and not its direction. We can then write (S.M. Flatté and T. Moody, manuscript in preparation, 1987):

$$\langle u(\theta) u(0) \rangle = 4\pi^2 k^2 \int_0^R dz \int_0^\infty K_T dK_T W(0, K_T, z) \sin^2 [K_T^2 z / 2k] J_0(K_T z \theta) \quad (23)$$

$$\langle \phi(\theta) \phi(0) \rangle = 4\pi^2 k^2 \int_0^R dz \int_0^\infty K_T dK_T W(0, K_T, z) \cos^2 [K_T^2 z / 2k] J_0(K_T z \theta) \quad (24)$$

$$\langle u(\theta) \phi(0) \rangle = 4\pi^2 k^2 \int_0^R dz \int_0^\infty K_T dK_T W(0, K_T, z) \sin [K_T^2 z / 2k] \cos [K_T^2 z / 2k] J_0(K_T z \theta) \quad (25)$$

Thus these angular correlation functions (ACFs) are very similar to the TCFs except that the transverse separation  $x_T$  has been replaced by  $z\theta$ ; in other words, the transverse separation is a linear function of depth, given by the separation of two rays

converging to the same point on the surface of the earth from the two different directions  $\theta_1$  and  $\theta_2$ . (See Figure 4.)

The normalized ACFs have at least two important properties: First, they provide another set of observables from array data that give a different weighting to inhomogeneities at different depths than the TCFs and hence provide further important constraints on medium models. Second, the variable  $\theta$  depends on having at least two sources; since there are many more source (earthquake) locations than there are stations in a typical seismic array and since these earthquakes provide angular differences down to fractions of a degree, the ACFs provide a much finer resolution of the medium inhomogeneities than the TCFs. For example, the NORSAR subarrays are separated by distances of 10 km or more, so that the transverse coherence for separations  $x_T$  smaller than about 10 km cannot be observed. However, observations with angular differences in incoming direction of about  $1^\circ$  are not uncommon, providing a probe of scales of 1 km even at a depth of 60 km.

Predictions for normalized ACFs for the medium spectrum of (22) (an exponential medium correlation function) are shown in Figure 3. Now the depth to which the medium extends becomes a more important factor in determining the curves. We see that the ACFs become narrower for media extending to larger depth if other parameters are kept the same.

#### 4. EXPERIMENTAL RESULTS

Previous results for the variances have been given by Aki [1973], Capon [1974], Berteussen *et al.*, [1975a, b], Powell and Meltzer [1984], and others. In many cases they presented their results in terms of a uniform, isotropic random layer with a Gaussian spectrum. We have inverted the relevant equations where necessary to revive their variance data with no imposition of a medium model. In cases where event-by-event results were given, we have averaged all the events presented. The results are given in Table 1. We see general agreement between the various determinations when expressed in this form, except for a few cases where a very small number of events were used. Variance results are graphed in Figure 2, where it is seen that individual events have a reasonably large scatter; averages are consistent with a power law type of medium rather than a Gaussian spectrum.

Previous results for TCFs were restricted to the log amplitude and phase without the cross-coherence TCF. Aki [1973] and Capon [1974] have presented approximate TCFs from LASA data showing decorrelation scales of the order of 10 km.

Previous results for ACFs consist only of qualitative comments. Berteussen [1975] remarks that events are well correlated in amplitude fluctuations if they are within a slowness difference of 0.5 s/deg, which implies that their incoming direc-

TABLE 1. Experimental Values for Variances

Reference	$\tau_{rms}, s$	$u_{rms}$	$\rho$
Aki [1973]	0.13	0.32	0.35
Capon [1974]	0.10	0.40	-
Berteussen <i>et al.</i> [1975a, b]	0.006–0.11	0.2–0.4	-
This work	0.135±0.004	0.410±0.006	0.26±0.03

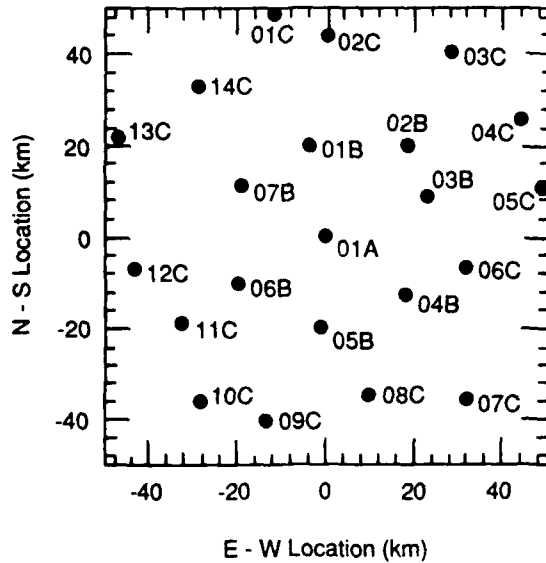


Fig. 5. Subarray spatial distribution at NORSAR. Subarray 01A is at latitude 60.82 N and longitude 10.83 E.

tions are within about  $2^\circ$  and gives an example showing that two events are substantially decorrelated if they are  $7^\circ$  apart in azimuth, which implies that their incoming directions are  $5^\circ$  apart.

There are many other publications that include attempts to fit a deterministic structure to the data from one or many events; we will not try to discuss their data, as it would have been presented in such a different way that the observations relevant to our attempts to observe small scale structure would not have been given. We discuss the relationship of our results to some of the deterministic results of others in section 6.

We now discuss our presentation of the NORSAR subarray data given in two NORSAR reports by Berteussen [1974] and Berteussen and Husebye [1974]. The data have been filtered in two important ways. First, a frequency filter has restricted the seismic frequency to 1–3 Hz, so the nominal center frequency is 2 Hz. Second, the elements within the subarrays have been added coherently; each subarray has about six elements spread over a circle of radius  $\sim 3.5$  km. The spatial distribution of subarrays is shown in Figure 5.

The travel time anomalies given by Berteussen [1974] are given for 104 beams; each beam is an average over a number of events whose source locations are close such that their incoming directions at the NORSAR array are within a few tenths of a degree. The travel time anomalies consist of arrival time residues with respect to a "best plane wave." We have removed the mean arrival time for each beam in our calculations. Figure 6 shows the arrival angle distribution of these beams.

The subarray intensity variations are given by Berteussen and Husebye [1974] for 185 beams. We have normalized these data such that for each beam the mean log amplitude is zero.

With this brief description of the gathering of the data (more details are given in the original reports) we now describe our method of estimating variances, TCFs and ACFs. More details, including our method of estimating the associated statistical errors, are given in the appendix.

If we had subarrays that were far apart and beams that were far apart in angle, then the information from each subarray and

from each beam would be statistically independent. The subarrays are far enough apart in location that they are reasonably independent for the purposes of error calculations. However, the beams are often close together, and hence the assumption of independent beams is not valid. If the beams are not independent, then the calculation of any quantity should use an appropriate weight for each beam. Let  $b$  be an index over the  $N$  beams; then we define  $w_b$  as the weight of beam  $b$ . The appendix describes our form for the weight. In order to calculate reasonable errors, we must establish the effective number of independent beams; this is also done in the appendix. We note that the number of independent beams is different for the different TCFs; we find 42.1, 11.5, and 32.4 for the effective number of independent beams in determining the TCFs of log amplitude, phase, and their cross-TCF, respectively. The ACFs have similar numbers, although the particular number varies with the angle.

To describe our formulas for the determination of experimental quantities, consider first the variances. We have

$$\langle u^2 \rangle = \frac{1}{N_w} \sum_{b=1}^N w_b \frac{1}{M} \sum_{s=1}^M (u_{bs})^2 \quad (26)$$

$$\langle \phi^2 \rangle = \frac{1}{N_w} \sum_{b=1}^N w_b \frac{1}{M} \sum_{s=1}^M (\phi_{bs})^2 \quad (27)$$

$$\langle u\phi \rangle = \frac{1}{N_w} \sum_{b=1}^N w_b \frac{1}{M} \sum_{s=1}^M (u_{bs}\phi_{bs}) \quad (28)$$

where  $b$  is an index over the  $N$  beams,  $N_w = \sum w_b$ , and  $s$  is an index over the  $M$  subarrays. The only difficulty in the above calculations is that the sets of beams for  $u$  and  $\phi$  are not identical. In order to calculate the cross coherence, we have searched through the two sets of beams and found corresponding pairs that are within  $1^\circ$  of each other and have considered them the same beam. The calculation of the errors is somewhat involved

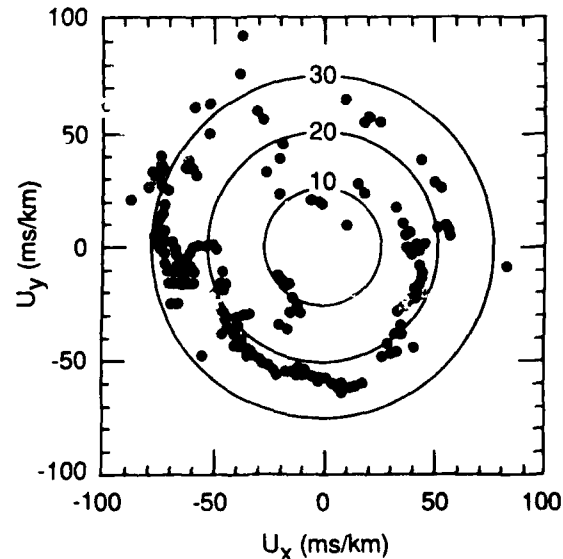


Fig. 6. Arrival angle distribution of the various beams defined at NORSAR. Each beam represents data from a cluster of earthquakes that are close enough that their seismic waves arrive at NORSAR with angles that are within a few tenths of a degree. The circles are labelled with the angle from the zenith in degrees. The axes are labelled with the components of slowness.

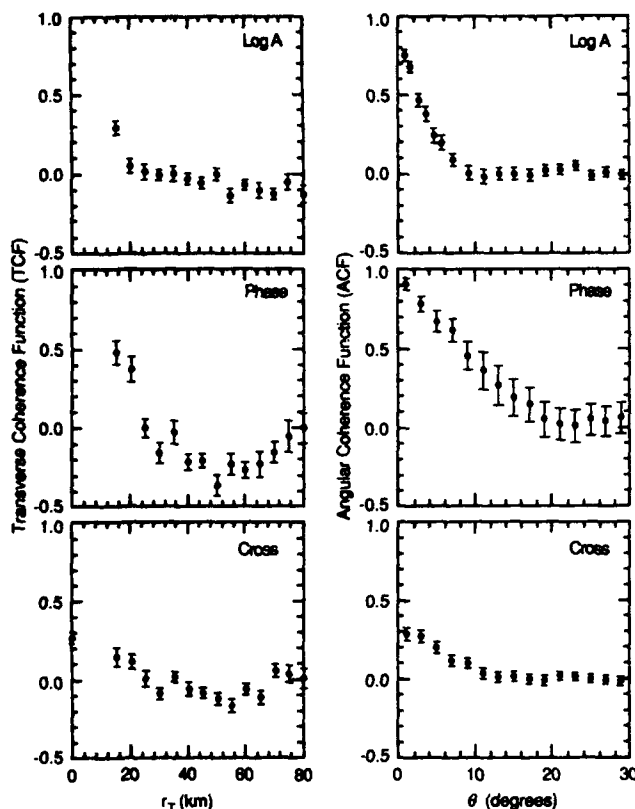


Fig. 7. Observed normalized TCFs and ACFs at NORSAR. Note that the regions of rapid variation in the TCFs are not covered well by the data, because the different subarrays have a minimum separation of about 15 km; the regions of rapid variation in the ACFs are well covered by the data, because the minimum separation in angle between the different beams is in the range of a few tenths of a degree.

and is given in the appendix. The results of the calculations of (26)–(28) are given in Table 1.

The TCFs are calculated with formulas analogous to (26)–(28). In order to plot a point at a transverse separation  $x_T$ , we include in the sum all pairs of elements with their separation  $x_T$  within a given bin. The results of this procedure are shown in Figure 7. We see that the smallest separation available is about 15 km, and the coherence is already below 0.5 at that separation.

Finally, we calculate the ACFs by the same method, with the order of summation reversed and with selection of pairs of beams whose angular difference is within a specified bin. The ACFs are also shown in Figure 7. We see that the experimental points in the ACFs have as much statistical precision and more resolution within the variable range for which there is significant variation in the coherence than the TCFs. The higher resolution of the ACFs compared with the TCFs follows from the closeness in arrival angle of the beams as compared to the spatial separation of the subarrays.

Certain dramatic features of the ACFs provide constraints on earth structure models. The phase coherence function has a smooth almost linear drop to a small coherence at an angle of about  $15^\circ$ . The log amplitude coherence has a distinctively different shape than the phase coherence; it drops sharply to 0.5 at an angle of about  $2^\circ$  but retains significant correlation out to angles of order  $10^\circ$ . We shall see in the next section the implications of these features for Earth models.

It is to be emphasized at this point that the nature of the NORSAR array restricts the scales of Earth structure that can be observed with NORSAR data. The approximate diameter of the array is 110 km. Because means and "best plane waves" have been subtracted from the data across the array, we cannot observe Earth structure with scales larger than about 110 km. Because the data consist of coherent addition of stations over subarrays that are about 7 km in diameter, we cannot observe structure with wavelengths smaller than about 5 km. Furthermore, our typical seismic wavelength at 2 Hz of 4 km also implies that we cannot observe structure wavelengths less than  $\sim 4$  km. These facts have to be taken into account in the theoretical models with which we compare the experimental data.

It is true that the separations of stations within subarrays are in the 1- to 7-km range. We have obtained station data for 13 nuclear explosion events of high signal-to-noise ratio at NORSAR. We have found that the station-by-station time anomalies are less than 0.1 s and are difficult to measure reliably because of the differing signal temporal structures. The signal intensities are more reliable; we have taken a 5-s time window at the start of the signal and have calculated the log amplitude TCF in the same manner that we did for the subarray data. The results will be shown later when we compare models to the data.

It is of interest to note that the results of this and the previous section, that is, the TCFs and the ACFs, can be used to understand the errors and possible biases of sparse arrays in measuring the magnitude of an earthquake or nuclear explosion. The analysis technique of *McLaughlin et al.* [1988], along with our experimentally determined coherence functions, could be applied to this problem.

## 5. SPECTRAL MODELS OF EARTH STRUCTURE UNDER NORSAR

We picture the crust, lithosphere, and asthenosphere below the Earth's surface as having random variations in seismic wave speed that are described by a spectrum that may depend on depth and may be anisotropic. We assume that the spectrum does not depend to first order on small changes in geographical position within the region under the NORSAR seismic array. The most desirable situation would be one in which we had enough experimental information to invert the data for all the characteristics of the spectrum describing these variations. We do not delude ourselves into thinking that our present data set is adequate for the task. However, we can impose some constraints on these type of models by analysis of the data, and we can find an Earth model which is at least consistent with the data and with what we know of the Earth's structure from other information.

We need to modify our theoretical expressions for the fact that the NORSAR array has a finite size and for the fact that the NORSAR data are averaged over subarrays and is at finite nonzero wavelength. The finite size is modeled by removing from the spectrum all wavelengths greater than 110 km. There is a considerable uncertainty in exactly where this upper wavelength cutoff should be because it depends on exactly how the "best plane waves" were removed and how averages of log amplitude were made; the main comment to make is that this cutoff should be arranged to fit the coherence functions at large separations; as a result the observed large-separation coherences are not a strong constraint on Earth models. This cutoff does not introduce artifacts into the coherence functions at small transverse separations or at small angular separations.

The subarray averaging might be modeled by assuming that the data are averaged uniformly over the area of a circle of radius  $r_o = 3.5$  km. This convolution corresponds in the spectral domain with multiplying our spectra by the following function of  $K_T$ :

$$C(K_T) \equiv \left[ \frac{2J_1(K_T r_o)}{K_T r_o} \right]^2 \quad (29)$$

This function has its first zero at  $K_T r_o = 3.8$ , or a medium-wavelength cutoff of 5.5 km. In our theoretical models we use a small-wavelength cutoff of 5.5 km. Again, this cutoff does not introduce artifacts into the coherence functions, but it does affect their exact shape at very small separations (of order 5 km or  $1^\circ$ ); future investigation of individual station waveforms will allow a more rigorous treatment of these cutoffs.

The first model we may try is one with an exponential correlation function with a scale length of 10 km, following those authors who have looked only at TCFs [Aki, 1973; Capon, 1974; Capon and Berteussen, 1974; Berteussen et al., 1975a, b; Powell and Melzer, 1984]. (See Figure 8.) We see that the TCF data and the ACF of phase are not badly fit with medium variations extending down to about 200 km, but the ACF of log amplitude and the cross ACF have significant disagreements between model and data. The disagreements have to do with the shapes of the ACFs in the regions of their rapid variations: at angles less than  $10^\circ$ . We should point out that disagreements at

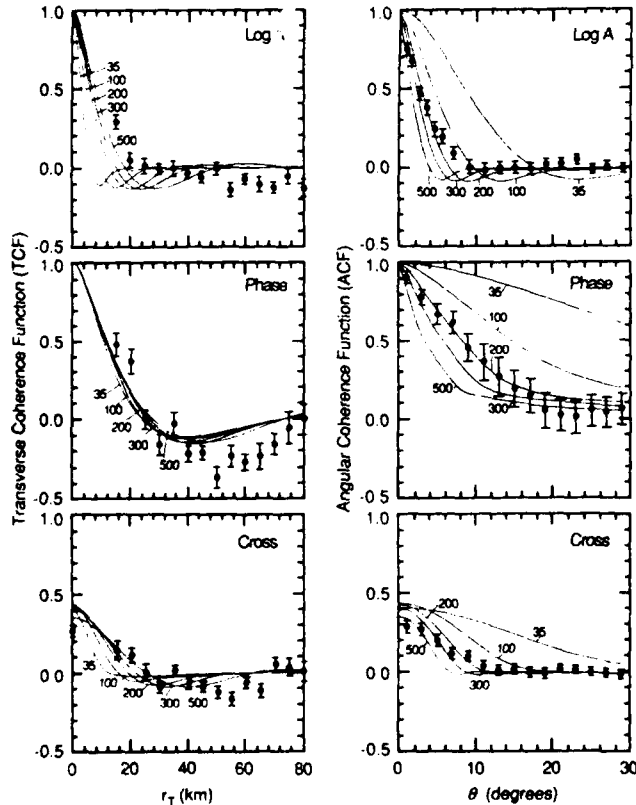


Fig. 8. Comparison between the data and calculations based on uniform random extended media with exponential correlation functions having a scale length of 10 km. The media extend from the surface to depths of 35 to 500 km. Note that the best medium extent for the ACF of phase is about 200 km, but that model does not give a good fit to the shapes of the ACF of log amplitude and the cross ACF.

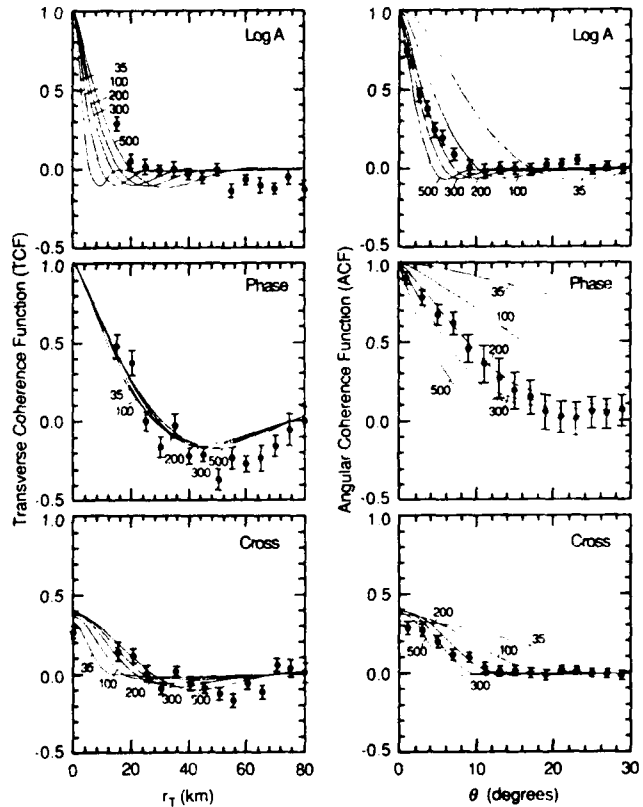


Fig. 9. Comparison between the data and calculations based on uniform random extended media with power-law spectra having index  $p = 3$  (self-similar). The media extend from the surface to depths of 35 to 500 km. As in Fig. 8, the best medium extent for the ACF of phase is about 200 km. This self-similar model gives a better fit than the exponential correlation model, but the self-similar model still does not fit the shapes of the ACF of log amplitude and the cross ACF.

large angles are probably less important because the shapes of the functions there are affected by the finite aperture of the NORSAR array. It is of interest even in this rather unsatisfactory model that structure is necessary down to several hundred kilometers to give a fit with reasonable average scale lengths.

The data in Figure 2 indicate that a power law spectrum is also appropriate for comparison to the data (in this case,  $\gamma$  and  $\rho$ ). We will therefore restrict further models to a particular type of spectrum: a power law expressed in the form

$$W(K) = AK^{-\gamma} \quad (30)$$

There is a wide variety of models with power law spectra because the power law index  $p$  may change with depth, as may the strength  $A$ . We have tried many examples of uniform media down to a cutoff depth, but none of the fits were judged to be acceptable. For example, Frankel and Clayton [1986] suggested the use of a uniform layer with a power law medium with  $p = 3$ , which they refer to as a self-similar medium. Figure 9 shows the predictions of such a medium; we see that the fit is better than that of the exponential medium, but some disagreements remain in the ACF of log amplitude and the cross ACF at angles less than  $10^\circ$ .

We have found one combination of power law media that we feel does fit the data reasonably well. We have not yet completed a full inversion to obtain a quantitative idea of the param-



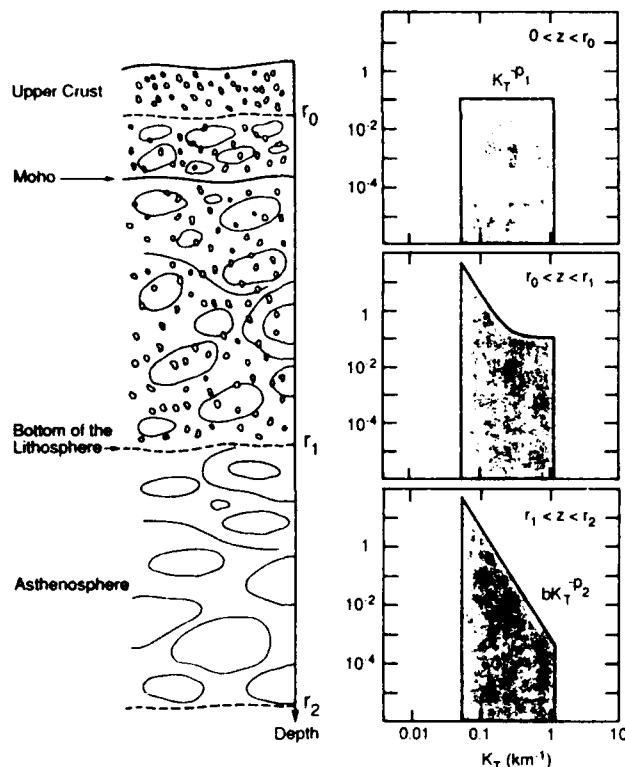


Fig. 10. Schematic representation of our best model of random variations under the NORSAR array. The model spectra have sharp cutoffs at low and high wave number to simulate the effects of the finite array aperture, the finite size of the subarrays, and the finite seismic wavelength.

eter uncertainties in this model. Our best model consists of two overlapping layers (Figure 10). The first layer from the surface down to 200-km depth has a power law index  $p = 0$ : in other words, a band-limited white spectrum. The second layer lies between depths of 15 and 250 km and has a power law index  $p = 4$  and a strength such that the  $p = 0$  and  $p = 4$  spectra cross at  $K = 0.31 \text{ km}^{-1}$ . Note that  $p = 4$  corresponds to the high wave number behavior of an exponential correlation function.

Comparison of the data and our best model is shown in Figure 11. One important feature of the data that constrains the model is the rapid decrease in the log amplitude ACF compared with the phase ACF. Most single-layer models have a similar shape for the two ACFs; in our best model, the log amplitude ACF is controlled by the shallow, flat spectrum layer, and the phase ACF is controlled by the deep, steep spectrum model.

Figure 12 shows the predictions of several variations on our best model: the shallow layer alone, the deep layer alone, the result of extending the shallow layer to 250 km instead of only 200 km, and the result of extending the deep layer up to the surface instead of only to 15-km depth. The fits are clearly inferior to the best model, although the differences of the latter two examples from our best fit model are not terribly striking.

The rms variations in phase and log amplitude are directly proportional to the rms variation in  $P$  wave velocity in our model. However, they are also proportional to the square root of the medium correlation length in the vertical, which we have not measured. If we assume that the medium spectrum is isotropic, then taking the observed rms value of  $u$  as 0.41, we deduce an

rms variation in  $P$  wave velocity of 0.9% in the upper layer and 0.5% in the lower layer. If we use the observed rms value of  $\phi$ , which is 1.70, we find values of 2.2 and 1.3%. We regard the difference between the values obtained from log amplitude variance and from arrival time variance as not very significant because the determination of overall variance, as opposed to spectral level, is notoriously difficult (Platté et al., 1979). The difference does imply that our result for rms  $P$  wave velocity fluctuation must be stated with large uncertainty; that is, it is between 1 and 4%, if an isotropic spectrum is assumed. However, it does not seem likely that isotropy is appropriate. If we define the anisotropy ratio as the horizontal correlation length over the vertical correlation length, then our result for the velocity fluctuation is proportional to the square root of that ratio. The fact that the upper and lower layers have rms variations within a factor of 2 of each other indicates that neither are second-order effects; both layers are significant in determining the wave fluctuations observed in the seismic array.

The predictions for the phase and cross TCFs fit the data reasonably well, but the log amplitude TCF prediction appears, mainly because of one data point, to decrease more rapidly than the data. After observing this discrepancy we used 13 nuclear explosion events at NORSAR to determine a more accurate experimental log amplitude TCF. (See section 4.) This TCF

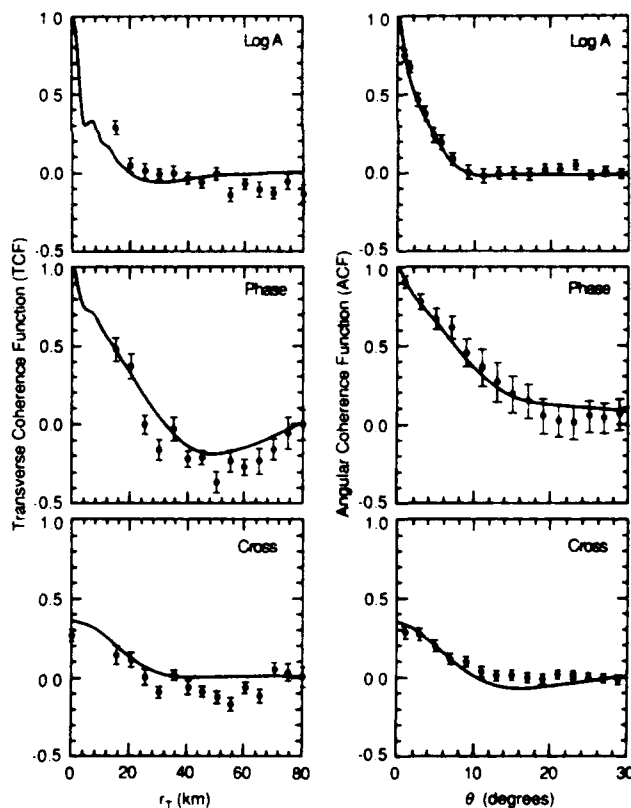


Fig. 11. Comparison between the data and the predictions of our best model, consisting of two overlapping layers. Each layer has a power law spectrum characterized by spectral index  $p$ . The characteristics of the two layers are  $(0 < z < 200 \text{ km}; p = 0)$  and  $(15 < z < 250 \text{ km}; p = 4)$  with normalization such that in the overlapping depth region they have equal spectral levels at wavenumber  $0.31 \text{ km}^{-1}$ . The fit is quite reasonable, particularly in the regions of rapid variation (less than  $10^\circ$  in the ACFs).

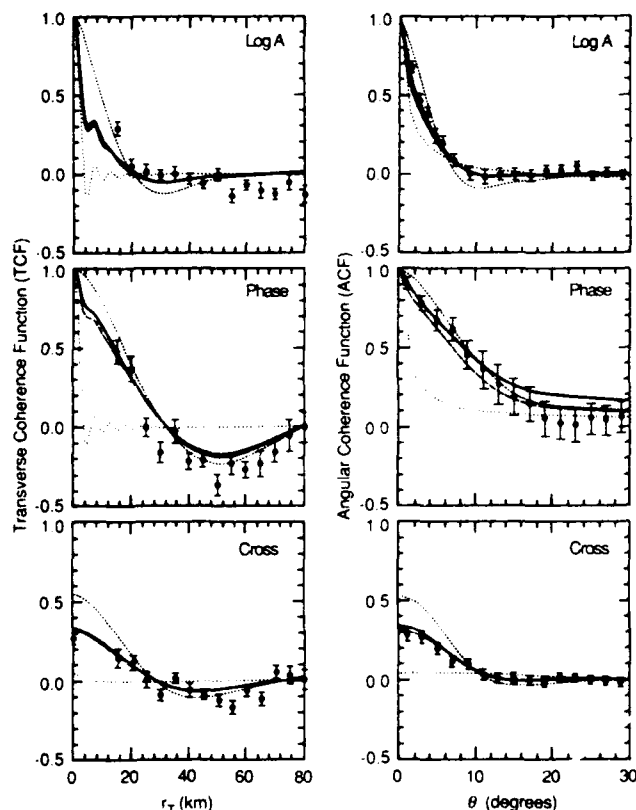


Fig. 12. Comparison between the data and the predictions for variations taken from our best model. Short dashes: the deep layer only; dotted: the shallow layer only; long dashes: our best model modified by extending the shallow layer to a depth of 250 km; solid: our best model modified by extending the deep layer up to the surface.

involves single seismometer stations rather than subarray averages and hence involves separations down to 3 km. We were gratified to observe the agreement between our best model prediction and this data set obtained after we had developed our best model mostly from the ACFs. (See Figure 13.)

#### 6. GEOPHYSICAL INTERPRETATION OF THE OBSERVED MEDIUM VARIATIONS

The Earth is characterized by vigorous geological activity driven by convection in the mantle. It is believed that most of the temperature increase with depth in the Earth occurs within thin boundary layers at the top and bottom of the mantle. But this is a statement about averages, and numerical simulations of mantle convection have indicated that strong variations may occur in these boundary layers [Boss and Sacks, 1985; Olson *et al.*, 1987]. These variations may involve temperature differences of up to 1000 K, with spatial scales perhaps comparable to the postulated boundary layer thicknesses of order 100 km. The variations may also involve compositional differences or, in the upper mantle, variations due to partial melting. Although there is a wide variety of possibilities for the formation of Earth inhomogeneities, we think it helpful to note that our observations can be interpreted as small-scale variations driven by dynamic mantle convection, or as fossilized compositional differences, perhaps induced by convective processes in earlier eras.

The change from the shallow layer with its abundant small-

scale structure to the deep layer with predominantly larger-scale variations could be indicative of some change in rock strength. One way to obtain small-scale structure is from a statistical distribution of cracks, but it seems unlikely that cracks would extend to 100-km depths. Another way would be to have a random distribution of relatively homogeneous layers with discontinuities in  $P$  wave speed from one layer to the next: layers whose thickness, horizontal extent, and wave speed discontinuity across interfaces are statistical in nature. Our results would imply that these random layers do not persist below about 200-km depth.

The rms variation in seismic wave speed that is implied by our spectral model is a few percent over the wavelength band 5.5–110 km, which is obtained from the variance of phase or log amplitude. This small variation, which has been obtained by previous workers as well, is not inconsistent with known properties of materials combined with the above geophysical parameters.

We may note some relationships of our results to previous studies of deterministic structure in the same depth regime. All of these studies deduced structure whose lateral variations are at scales larger than 100 km. Our data discriminate against structure with lateral wavelengths greater than 110 km. Therefore our results are complementary to the following deterministic studies, whose results should in some cases be geologically related to ours.

Haddon and Husebye [1978] constructed a model with a single, deep dipping layer (thin lens model), calculated its predictions by the parabolic wave equation, and compared them with the spatial structure of arrival time and amplitude across the NORSAR array. They concluded that a layer at a depth of 150–200 km explains a good fraction of the variances. Their

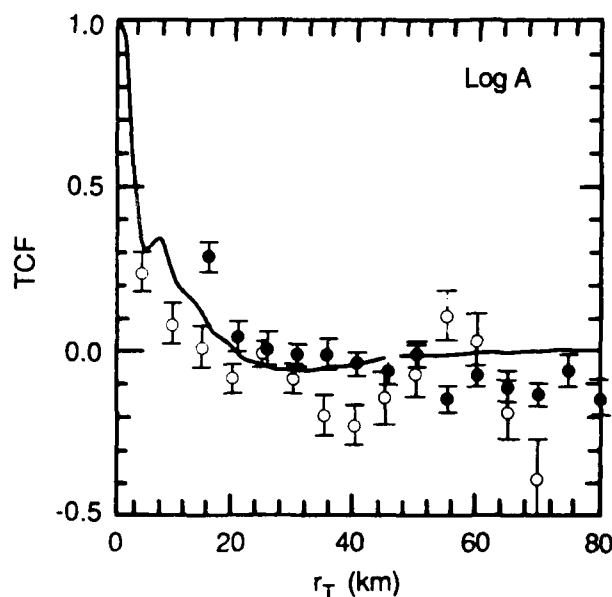


Fig. 13. The TCF of log amplitude for 13 nuclear explosion events (eight from the Soviet Union, five from the United States) detected at NORSAR (open circles). The data were calculated from individual station waveforms; note that the individual stations have separations that range down to about 3 km. We see that when the resolution is available, the coherence function drops to less than 0.5 in a few kilometers. For comparison, the solid circles are the same points shown in Figure 7, which represent subarray-averaged data.

amplitude data had been smoothed such that only the large-scale systematic variation was kept. Therefore their results are complementary to ours.

Sacks *et al.* [1979] deduce a discontinuity at 250 km from observations of long-period precursors to direct *S* at NORSAR. They suggest the precursors result from *S* to *P* conversion at the discontinuity, which they assume to be the lithosphere-asthenosphere boundary. Our results also show that 250 km is an interesting depth. We would rather favor the interpretation that 250 km is the bottom of a thermal boundary layer in the mantle, with the bottom of the lithosphere being at 200 km.

Given and Helmberger [1980] deduce laterally independent structure of *P* wave velocity as a function of depth for northwest Eurasia, using short-period and long-period body waves from nuclear explosions. They see a low-velocity zone in the regime of 150–200 km, which is likely to be geologically related to our observations of changes at 200 and 250 km.

Husebye *et al.* [1986] reported a seismic tomographic survey of the lithosphere-asthenosphere beneath southern Scandinavia using travel time residuals. They placed the boundary between the lithosphere and asthenosphere between 100 and 200 km, with lateral variations of scale greater than 100 km.

Thus other studies of the larger-scale lateral variations under NORSAR have indicated structure at depths of 150–250 km, which should be combined with our observations of smaller-scale lateral variations down to the same depth range in order to create a geologically consistent picture.

Present ability to model the detailed dynamics of mantle convection is so crude that as yet no meaningful comparison between the strength and spectrum of variations that we observe and the expected product of mantle convection is possible. However, one can hope that future understanding of mantle convection, perhaps involving numerical simulation, will be influenced by measurements such as ours of the strength and spectrum of seismic wave speed variations in the thermal boundary layers of the mantle. More generally, improved geological understanding of the crust and lithosphere may come from requiring agreement with the small-scale variations that we observe in our shallow layer.

#### APPENDIX

##### TCFs and Their Statistical Errors

We begin the treatment of error estimates for the TCFs by considering the expression for the TCF of log amplitude obtained from the data of one beam:

$$c_b(x_T) = \frac{1}{M} \sum_{p=1}^M u_{bs} u_{bt} \quad (\text{A1})$$

where *p* is an index over the *M* pairs of subarrays whose separation is within the desired bin of *x<sub>T</sub>*. (The index of the first member of the pair is *s*; the index of the second member is *t*.) The approximate variance of *c<sub>b</sub>* is obtained as follows: First, the expectation value of *c<sub>b</sub>* is needed,

$$\langle c_b \rangle = \rho_i(x_T) \quad (\text{A2})$$

where *ρ<sub>i</sub>* is the unnormalized TCF at *x<sub>T</sub>*. Next, the expectation value of the square is needed,

$$\langle c_b^2 \rangle = \frac{1}{M^2} \sum_p \sum_q \langle u_{bs} u_{bt} u_{qs} u_{qt} \rangle \quad (\text{A3})$$

Our assumption of Gaussian variables allows us to evaluate the above fourth moment in terms of all possible permutation of

products of second moments [Flatté *et al.*, 1979]. The result is then

$$\langle c_b^2 \rangle = \rho_i^2 + \frac{1}{M} \langle u^2 \rangle^2 \quad (\text{A4})$$

where we have ignored many of the off-diagonal coherences as small compared with the variance of *u*. Thus the variance of *c<sub>b</sub>* is

$$\sigma_b^2 = \frac{1}{M} \langle u^2 \rangle^2 \quad (\text{A5})$$

It is important to note that because we have many beams, we can observe *σ<sub>b</sub>* at each *x<sub>T</sub>*. We simply plot the distribution of *c<sub>b</sub>* from the many beams and calculate the variance of the distribution. The question is, what is the uncertainty in *c<sub>b</sub>* after combining all the information from the many beams? We will couch this in the form of the question of determining *N<sub>eff</sub>*, the effective number of independent beams.

Since we have data from *N* beams, we should combine them in an appropriate manner, that is, with weights:

$$c(x_T) \equiv \langle u(x_T) u(0) \rangle = \frac{1}{N_w} \sum_{b=1}^N w_b c_b(x_T) \quad (\text{A6})$$

where *b* is an index over the *N* beams, *w<sub>b</sub>* is the weight assigned to each beam, and

$$N_w = \sum_{b=1}^N w_b \quad (\text{A7})$$

If the *N* beams were independent, then the optimal combination would require *w<sub>b</sub>* = 1, and it is simple to show that the variance of *c* is given by

$$\sigma^2 = \frac{1}{NM} \langle u^2 \rangle^2 \quad (\text{A8})$$

We define the number of effective beams as

$$N_{\text{eff}} \equiv \frac{\sigma_b^2}{\sigma^2} \quad (\text{A9})$$

That is, in order to calculate the variance of our measurement of the TCF at a particular *x<sub>T</sub>*, we observe the distribution of that TCF from our many beams, determine its variance from that distribution, and then divide by *N<sub>eff</sub>*. For the case of independent beams, from (A5) and (A8) we see that *N<sub>eff</sub>* is equal to the total number of beams *N*.

However, many of the beams in this data set are so close to each other that the information in each is not independent. Therefore a more accurate measure of the TCF is obtained by weighting each beam by a number smaller than unity if there are nearby similar beams. We have chosen weights for each beam in the following way:

$$w_b = \frac{1}{N \left( 1 + \sum_{d \neq b} \rho_a(\theta_{bd}) \right)} \quad (\text{A10})$$

where *ρ<sub>a</sub>*(*θ<sub>bd</sub>*) is the ACF between beams and *θ<sub>bd</sub>* is the angle between beam *b* and beam *d*. This weighting has the appropriate limits; first, it is equal to unity if all beams are far from each other and therefore independent; second, if there are *n* beams on top of each other, each beam has a weight of 1/*n*.

Now we must estimate the statistical error on this coherence function. We emphasize that our treatment of errors makes significant approximations; it is very difficult to be more accu-

rate in the evaluation of errors without going through an extensive program of numerical simulation. We assume that all the beams are in a narrow cone, so that the expectation value of the TCF for each beam is the same, and we assume that the statistics of the log amplitude or arrival time are close enough to Gaussian to estimate the error reasonably. Let us use a shorthand notation in which  $x_T$  is suppressed:

$$c = \frac{1}{N_w} \sum_{b=1}^N w_b c_b \quad (\text{A11})$$

and we need to find an appropriate expression for  $\langle c^2 \rangle$ .

$$\langle c^2 \rangle = \frac{1}{N_w^2} \sum_{b=1}^N \sum_{d=1}^N w_b w_d \langle c_b c_d \rangle \quad (\text{A12})$$

But each  $c_b$  is the sum of products of two log amplitudes. We may indicate this by

$$\langle c_b c_d \rangle = \frac{1}{M^2} \sum_{i=1}^M \sum_{j=1}^M \langle u(x_i, \theta_b) u(y_j, \theta_b) u(x_j, \theta_d) u(y_i, \theta_d) \rangle \quad (\text{A13})$$

where  $x_{i,j}$  and  $y_{i,j}$  are separated in space by  $x_T$  and  $\theta_b$  is the angle of beam  $b$ . Thus we need to evaluate a fourth moment of log amplitude. The Gaussian assumption provides us with the means; in the Gaussian case the fourth moment is the sum of all possible permutations of products of second moments [Flatté *et al.*, 1979]. Consider first the permutation in which the pair of  $u$  from beam  $b$  and the pair of  $u$  from beam  $d$  are kept together. Each pair has an expectation value of  $\rho_i$ , and the entire contribution of that permutation consists of  $\rho_i^2$ . The other permutations involve second moments with one  $u$  from beam  $b$  and one  $u$  from beam  $d$ . We consider only the contributions for those pairs of  $u$  that are at the same station, since other pairs will have a substantially smaller coherence. It then follows that

$$\langle c^2 \rangle = \rho_i^2 + \frac{1}{N_w^2} \sum_{b=1}^N \sum_{d=1}^N w_b w_d \frac{\rho_d^2(\theta_{bd})}{M} \quad (\text{A14})$$

and that the variance of  $c$  is

$$\sigma^2 = \frac{1}{N_w^2} \sum_{b=1}^N \sum_{d=1}^N w_b w_d \frac{\rho_d^2(\theta_{bd})}{M} \quad (\text{A15})$$

The effective number of beams is then determined from (A5), (A9), and (A15) to be

$$N_{\text{eff}}^{-1} = \frac{1}{N_w^2} \sum_{b=1}^N \sum_{d=1}^N w_b w_d \frac{\rho_d^2(\theta_{bd})}{\langle u^2 \rangle^2} \quad (\text{A16})$$

and we note that the last ratio is just what we call the normalized ACF. We can use our measurements of the normalized ACF to evaluate  $N_{\text{eff}}$  for each point on the TCF, and our measurements of the values of  $c_b$  for the different beams to evaluate the variance of  $c_b$ . Finally, we apply (A9) to find  $\sigma$ . The above procedure is easily applied to the other two TCFs as well.

#### ACFs and Their Statistical Errors

The above principles also apply to the problem of evaluating the ACFs and their errors. In the ACF case the fundamental measurement requires a pair of beams instead of the single beam of the TCF case. In establishing the weights, we ask whether a given pair is independent of another pair. Furthermore, when we form a fourth moment of a quantity, we are dealing with four beams instead of two.

Our procedure for forming the weights is as follows: First, we find all pairs of beams that are separated by a desired angle  $\theta$ . Then the weight for pair  $q$  is given by

$$w_q^{-1} = 1 + \sum_{p \neq q} \rho_p(\theta_1) \rho_p(\theta_2) \quad (\text{A17})$$

where the sum is over all the other pairs. The angles  $\theta_1$  and  $\theta_2$  are chosen so that the product of the  $\rho$ 's is the maximum. Again, this form has the correct limiting values.

The expression for the ACF can be given then as

$$\rho_s(\theta) = \frac{1}{N_w} \sum_{p=1}^N w_p \frac{1}{M} \sum_{r=1}^M u_{pq} u_{rs} \quad (\text{A18})$$

where  $q$  and  $r$  are the indices of the beams making up pair  $p$  and  $s$  is the index of the station within the array. In evaluating the fourth moment as a product of second moments, we again treat the first permutation completely and then ignore those pairs which belong to different stations in subsequent permutations. We find

$$N_{\text{eff}}^{-1} = \frac{1}{N_w^2} \sum_p \sum_q w_p w_q \rho_{pq}(\phi) \rho_{pq}(\psi) \quad (\text{A19})$$

where  $p$  and  $q$  are different beam pairs with angle difference  $\theta$  and  $\rho_{pq}$  is the normalized ACF. The angle  $\phi$  is the smallest angle obtained by selecting one beam from each of the two beam pairs. The angle  $\psi$  is the angle between the other two beams. Again, this is an approximation, which has the right behavior in the limiting case of many beam pairs, each of which is made up of the same beams.

It is of interest to point out that within our approximations, the values of a TCF at different  $x_T$  and the values of an ACF at different  $\theta$  are not correlated.

**Acknowledgments.** We are grateful for discussions with Zheng-Kang Shen. This work was supported by Defense Advanced Research Projects Agency grant MDA903-86-K-0010.

#### REFERENCES

- Aki, K. Scattering of P waves under the Montana Lasa, *J. Geophys. Res.*, 78, 1334-1346, 1973.
- Aki, K. Scattering and attenuation of shear waves in the lithosphere, *J. Geophys. Res.*, 85, 6496-6504, 1980.
- Aki, K., Source and scattering effects on the spectra of small local earthquakes, *Bull. Seismol. Soc. Am.*, 71, 1687-1700, 1981.
- Aki, K. and A.B. Chouet, Origin of coda waves: Source, attenuation and scattering effects, *J. Geophys. Res.*, 80 3322-3342, 1975.
- Bergmann, P.G., Propagation of radiation in a medium with random inhomogeneities, *Phys. Rev.*, 70, 486, 1946.
- Berteussen, K.A., NORSAR location calibrations and time delay corrections, *NORSAR Sci. Rep. 2-73/74*, National Technical Information Service, Springfield, Va., 1974.
- Berteussen, K.A., P wave amplitude variability at NORSAR, *J. Geophys.*, 41, 595-613, 1975.
- Berteussen, K.A., A. Christofferson, E.S. Husebye and A. Dahle, Wave scattering theory in analysis of P wave anomalies at NORSAR and LASA, *Geophys. J. R. Astron. Soc.*, 42, 403-417, 1975a.
- Berteussen, K.A., and E.S. Husebye, Amplitude pattern effects on NORSAR P wave detectability, *NORSAR Sci. Rep. 1-74/75*, National Technical Information Service, Springfield, Va., 1974.
- Berteussen, K.A., E.S. Husebye, R.F. Meres, and A. Ram Quantitative assessment of the crust-upper mantle heterogeneities beneath the Gauribidanur seismic array in southern India, *Earth Planet. Sci. Lett.*, 37, 326-332, 1975b.
- Boss, A.P. and I.S. Sacks, Formation and growth of deep mantle plumes, *Geophys. J. R. Astron. Soc.*, 80, 241-255, 1985.
- Capon, J., Characterization of crust and upper mantle structure under Lasa as a random medium, *Bull. Seismol. Soc. Am.*, 64, 235-266, 1974.
- Capon, J., and K.A. Berteussen, A random medium analysis of crust and upper mantle structure under NORSAR, *Geophys. Res. Lett.*, 1, 327-328, 1974.

- Chernov, L.A., *Wave Propagation in a Random Medium*, McGraw-Hill, New York, 1960.
- Dashen, R., Path integrals for waves in random media, *J. Math. Phys.*, **20**, 894-920, 1979.
- Dashen, R., S.M. Flatté, and S.A. Reynolds, Path-integral treatment of acoustic mutual coherence functions for rays in a sound channel, *J. Acoust. Soc. Am.*, **77**, 1716-1722, 1985.
- Fante, R.L., Electromagnetic beam propagation in turbulent media: an update, *Proc. IEEE*, **68**, 1424-1443, 1980.
- Flatté, S.M., Wave propagation through random media: contributions from ocean acoustics, *Proc. IEEE*, **71**, 1267-1294, 1983.
- Flatté, S.M. and R.B. Stoughton, Theory of acoustic measurement of internal-wave strength as a function of depth, horizontal position, and time, *J. Geophys. Res.*, **91**, 7709-7720, 1986.
- Flatté, S.M., R. Dashen, W.H. Munk, K.M. Watson, and F. Zachariassen, *Sound Transmission Through a Fluctuating Ocean*, Cambridge University Press, New York, 1979.
- Flatté, S.M., S.A. Reynolds, and R. Dashen, Path-integral treatment of intensity and intensity moments for rays in a sound channel, *J. Acoust. Soc. Am.*, **82**, 967-972, 1987a.
- Flatté, S.M., S.A. Reynolds, R. Dashen, B. Buehler, and P. Maciejewski, AFAR measurements of intensity and intensity moments, *J. Acoust. Soc. Am.*, **82**, 973-980, 1987b.
- Fock, V.A., Theory of radio-wave propagation in an inhomogeneous atmosphere for a raised source, *Izv. Akad. Nauk. SSSR, Ser. Fiz.*, **14**, 70, 1950.
- Frankel, A., and R.W. Clayton, Finite-difference simulations of seismic scattering: Implications for the propagation of short-period seismic waves and models of crustal inhomogeneity, *J. Geophys. Res.*, **91**, 6465-6489, 1986.
- Garrett, C., and W.H. Munk, Space-time scales of internal waves: A progress report, *J. Geophys. Res.*, **80**, 291-297, 1975.
- Given, J.W., and D.V. Helmberger, Upper mantle structure of northwestern Eurasia, *J. Geophys. Res.*, **85**, 7183-7194, 1980.
- Haddon, R.A.W., and E.S. Husebye, Joint interpretation of *P* wave time and amplitude anomalies in terms of lithospheric heterogeneities, *Geophys. J. R. Astron. Soc.*, **55**, 19-43, 1978.
- Husebye, E.S., J. Hovland, A. Christofferson, K. Astrom, R. Slunga, and C.-E. Lund, Tomographical mapping of the lithosphere and asthenosphere beneath southern Scandinavia and adjacent areas, *Tectonophysics*, **128**, 229-250, 1986.
- Ishimaru, A., Theory and application of wave propagation and scattering in random media, *J. Proc. IEEE*, **65**, 1030-1061, 1977.
- Leontovich, M., and V. Fock, Solution of the problem of propagation of electromagnetic waves along the Earth's surface by the parabolic equation method, *J. Zh. Eksp. Teor. Fiz.*, **16**, 557-73, 1946.
- McLaughlin, K.L., T.W. McElfresh, and R.H. Shumway, Determination of event magnitudes with correlated data and censoring: A maximum likelihood approach, *Geophys. J. R. Astron. Soc.*, in press, 1988.
- Mintzer, D., Wave propagation in a randomly inhomogeneous medium, *J. Acoust. Soc. Am.*, **25**, 922-927, 1953.
- Munk, W.H. and F. Zachariassen, Sound propagation through a fluctuating ocean - Theory and observation, *J. Acoust. Soc. Am.*, **59**, 818-838, 1976.
- Olson, P., G. Schubert, and C. Anderson, Plume formation in the D''-layer and the roughness of the core-mantle boundary, *Nature*, **327**, 409-413, 1987.
- Powell, C.A., and A.S. Meltzer, Scattering of *P* waves beneath SCAR-LET in southern California, *Geophys. Res. Lett.*, **11**, 481-484, 1984.
- Prokhorov, A.M., F.V. Bunkin, K.S. Gochelashvili, and V.I. Shishov, Laser irradiance propagation in turbulent media, *Proc. IEEE*, **63**, 790-811, 1975.
- Reynolds, S.A., S.M. Flatté, R. Dashen, B. Buehler, and P. Maciejewski, AFAR measurements of acoustic mutual coherence functions of time and frequency, *J. Acoust. Soc. Am.*, **77**, 1723-1731, May 1985.
- Sacks, I.S., J.A. Snoke, and E.S. Husebye, Lithosphere thickness beneath the Baltic Shield, *Tectonophysics*, **56**, 101-110, 1979.
- Sato, H., Attenuation of *S* waves in the lithosphere due to scattering by its random velocity structure, *J. Geophys. Res.*, **87**, 7779-7785, 1982.
- Stoughton, R.B., S.M. Flatté, and B. Howe, Acoustic measurements of internal-wave rms displacement and rms horizontal current off Bermuda in late 1983, *J. Geophys. Res.*, **91**, 7721-7732, 1986.
- Strohbehn, J. W. (Ed.), *Laser Beam Propagation in the Atmosphere*, Springer-Verlag, New York, 1978.
- Tatarskii, V.I., *The Effects of the Turbulent Atmosphere on Wave Propagation*, National Technical Information Service, Springfield, Va., 1971.
- Tatarskii, V.I., and V.U. Zavorotnyi, Strong fluctuations in light propagation in a randomly inhomogeneous medium, *Progr. Opt.*, **18**, 204-256, 1980.
- Wang, T.I., G.R. Ochs, and S.F. Clifford, A saturation-resistant optical scintillometer to measure  $C_n^2$ , *J. Opt. Soc. Am.*, **68**, 334-338, 1978.
- Wu, R.S., Attenuation of short period seismic waves due to scattering, *Geophys. Res. Lett.*, **9**, 9-12, 1982.
- Wu, R.S., and K. Aki, The fractal nature of the inhomogeneities in the lithosphere evidenced from seismic wave scattering, *Pure Appl. Geophys.*, **123**, 805-818, 1985a.
- Wu, R.S., and K. Aki, Elastic wave scattering by a random medium and the small scale inhomogeneities in the lithosphere, *J. Geophys. Res.*, **90**, 10261-10273, 1985b.

S.M. Flatté and R.-S. Wu, Physics Department, University of California, Santa Cruz, CA 95064.

(Received November 11, 1987;  
revised February 22, 1988;  
accepted January 24, 1988.)

CONTRACTORS (United States)

Professor Keiti Aki  
Center for Earth Sciences  
University of Southern California  
University Park  
Los Angeles, CA 90089-0741

Professor Charles B. Archambeau  
Cooperative Institute for Resch  
in Environmental Sciences  
University of Colorado  
Boulder, CO 80309

Dr. Thomas C. Bache Jr.  
Science Applications Int'l Corp.  
10210 Campus Point Drive  
San Diego, CA 92121 (2 copies)

Dr. Douglas R. Baumgardt  
Signal Analysis & Systems Div.  
ENSCO, Inc.  
5400 Port Royal Road  
Springfield, VA 22151-2388

Dr. Jonathan Berger  
Institute of Geophysics and  
Planetary Physics  
Scripps Institution of Oceanography  
A-025  
University of California, San Diego  
La Jolla, CA 92093

Dr. S. Bratt  
Science Applications Int'l Corp.  
10210 Campus Point Drive  
San Diego, CA 92121

Dr. Lawrence J. Burdick  
Woodward-Clyde Consultants  
P.O. Box 93245  
Pasadena, CA 91109-3245 (2 copies)

Professor Robert W. Clayton  
Seismological Laboratory/Div. of  
Geological & Planetary Sciences  
California Institute of Technology  
Pasadena, CA 91125

Dr Karl Coyner  
N. E. Research  
P.O. Box 857  
Norwich, VT 05055

Dr. Vernon F. Cormier  
Department of Geology & Geophysics  
U-45, Room 207  
The University of Connecticut  
Storrs, Connecticut 06268

Dr. Steven Day  
Dept. of Geological Sciences  
San Diego State U.  
San Diego, CA 92182

Dr. Zoltan A. Der  
ENSCO, Inc.  
5400 Port Royal Road  
Springfield, VA 22151-2388

Professor John Ferguson  
Center for Lithospheric Studies  
The University of Texas at Dallas  
P.O. Box 830688  
Richardson, TX 75083-0688

Professor Stanley Flatte'  
Applied Sciences Building  
University of California,  
Santa Cruz, CA 95064

Dr. Alexander Florence  
SRI International  
333 Ravenswood Avenue  
Menlo Park, CA 94025-3493

Professor Steven Grand  
Department of Geology  
245 Natural History Building  
1301 West Green Street  
Urbana, IL 61801

Dr. Henry L. Gray  
Associate Dean of Dedman College  
Department of Statistical Sciences  
Southern Methodist University  
Dallas, TX 75275

Professor Roy Greenfield  
Geosciences Department  
403 Deike Building  
The Pennsylvania State University  
University Park, PA 16802

Professor David G. Harkrider  
Seismological Laboratory  
Div of Geological & Planetary Sciences  
California Institute of Technology  
Pasadena, CA 91125

Professor Donald V. Helmberger  
Seismological Laboratory  
Div of Geological & Planetary Sciences  
California Institute of Technology  
Pasadena, CA 91125

Professor Eugene Herrin  
Institute for the Study of Earth  
and Man/Geophysical Laboratory  
Southern Methodist University  
Dallas, TX 75275

Professor Robert B. Herrmann  
Department of Earth & Atmospheric  
Sciences  
Saint Louis University  
Saint Louis, MO 63156

Professor Bryan Isacks  
Cornell University  
Dept of Geological Sciences  
SNEE Hall  
Ithaca, NY 14850

Professor Lane R. Johnson  
Seismographic Station  
University of California  
Berkeley, CA 94720

Professor Thomas H. Jordan  
Department of Earth, Atmospheric  
and Planetary Sciences  
Mass Institute of Technology  
Cambridge, MA 02139

Dr. Alan Kafka  
Department of Geology &  
Geophysics  
Boston College  
Chestnut Hill, MA 02167

Professor Leon Knopoff  
University of California  
Institute of Geophysics  
& Planetary Physics  
Los Angeles, CA 90024

Professor Charles A. Langston  
Geosciences Department  
403 Deike Building  
The Pennsylvania State University  
University Park, PA 16802

Professor Thorne Lay  
Department of Geological Sciences  
1006 C.C. Little Building  
University of Michigan  
Ann Arbor, MI 48109-1063

Dr. Randolph Martin III  
New England Research, Inc.  
P.O. Box 857  
Norwich, VT 05055

Dr. Gary McCartor  
Mission Research Corp.  
735 State Street  
P.O. Drawer 719  
Santa Barbara, CA 93102 (2 copies)

Professor Thomas V. McEvilly  
Seismographic Station  
University of California  
Berkeley, CA 94720

Dr. Keith L. McLaughlin  
S-CUBED,  
A Division of Maxwell Laboratory  
P.O. Box 1620  
La Jolla, CA 92038-1620

Professor William Menke  
Lamont-Doherty Geological Observatory  
of Columbia University  
Palisades, NY 10964

Professor Brian J. Mitchell  
Department of Earth & Atmospheric  
Sciences  
Saint Louis University  
Saint Louis, MO 63156

Mr. Jack Murphy  
S-CUBED  
A Division of Maxwell Laboratory  
11800 Sunrise Valley Drive  
Suite 1212  
Reston, VA 22091 (2 copies)

Professor J. A. Orcutt  
Institute of Geophysics and Planetary  
Physics, A-205  
Scripps Institute of Oceanography  
Univ. of California, San Diego  
La Jolla, CA 92093

Professor Keith Priestley  
University of Nevada  
Mackay School of Mines  
Reno, NV 89557

Professor Paul G. Richards  
Lamont-Doherty Geological  
Observatory of Columbia Univ.  
Palisades, NY 10964

Wilmer Rivers  
Teledyne Geotech  
314 Montgomery Street  
Alexandria, VA 22314

Dr. Alan S. Ryall, Jr.  
Center of Seismic Studies  
1300 North 17th Street  
Suite 1450  
Arlington, VA 22209-2308 (4 copies)

Professor Charles G. Sammis  
Center for Earth Sciences  
University of Southern California  
University Park  
Los Angeles, CA 90089-0741

Professor Christopher H. Scholz  
Geological Sciences  
Lamont-Doherty Geological Observatory  
Palisades, NY 10964

Dr. Jeffrey L. Stevens  
S-CUBED,  
A Division of Maxwell Laboratory  
P.O. Box 1620  
La Jolla, CA 92038-1620

Professor Brian Stump  
Institute for the Study of Earth & Man  
Geophysical Laboratory  
Southern Methodist University  
Dallas, TX 75275

Professor Ta-liang Teng  
Center for Earth Sciences  
University of Southern California  
University Park  
Los Angeles, CA 90089-0741

Dr. Clifford Thurber  
State University of New York at  
Stony Brooks  
Dept of Earth and Space Sciences  
Stony Brook, NY 11794-2100

Professor M. Nafi Toksoz  
Earth Resources Lab  
Dept of Earth, Atmospheric and  
Planetary Sciences  
Massachusetts Institute of Technology  
42 Carleton Street  
Cambridge, MA 02142

Professor Terry C. Wallace  
Department of Geosciences  
Building #11  
University of Arizona  
Tucson, AZ 85721

Weidlinger Associates  
ATTN: Dr. Gregory Wojcik  
4410 El Camino Real, Suite 110  
Los Altos, CA 94022

Professor Francis T. Wu  
Department of Geological Sciences  
State University of New York  
at Binghamton  
Vestal, NY 13901



OTHERS (United States)

Dr. Monem Abdel-Gawad  
Rockwell Internat'l Science Center  
1049 Camino Dos Rios  
Thousand Oaks, CA 91360

Professor Shelton S. Alexander  
Geosciences Department  
403 Deike Building  
The Pennsylvania State University  
University Park, PA 16802

Dr. Ralph Archuleta  
Department of Geological  
Sciences  
Univ. of California at  
Santa Barbara  
Santa Barbara, CA

Dr. Muawia Barazangi  
Geological Sciences  
Cornell University  
Ithaca, NY 14853

J. Barker  
Department of Geological Sciences  
State University of New York  
at Binghamton  
Vestal, NY 13901

Mr. William J. Best  
907 Westwood Drive  
Vienna, VA 22180

Dr. N. Biswas  
Geophysical Institute  
University of Alaska  
Fairbanks, AK 99701

Dr. G. A. Bollinger  
Department of Geological Sciences  
Virginia Polytechnical Institute  
21044 Derring Hall  
Blacksburg, VA 24061

Dr. James Bulau  
Rockwell Int'l Science Center  
1049 Camino Dos Rios  
P.O. Box 1085  
Thousand Oaks, CA 91360

Mr. Roy Burger  
1221 Serry Rd.  
Schenectady, NY 12309

Dr. Robert Burridge  
Schlumberger-Doll Resch Ctr.  
Old Quarry Road  
Ridgefield, CT 06877

Science Horizons, Inc.  
ATTN: Dr. Theodore Cherry  
710 Encinitas Blvd., Suite 101  
Encinitas, CA 92024 (2 copies)

Professor Jon F. Claerbout  
Professor Amos Nur  
Dept. of Geophysics  
Stanford University  
Stanford, CA 94305 (2 copies)

Dr. Anton W. Dainty  
AFGL/LWH  
Hanscom AFB, MA 01731

Professor Adam Dziewonski  
Hoffman Laboratory  
Harvard University  
20 Oxford St.  
Cambridge, MA 02138

Professor John Ebel  
Dept of Geology & Geophysics  
Boston College  
Chestnut Hill, MA 02167

Dr. Donald Forsyth  
Dept. of Geological Sciences  
Brown University  
Providence, RI 02912

Dr. Anthony Gangi  
Texas A&M University  
Department of Geophysics  
College Station, TX 77843

Dr. Freeman Gilbert  
Institute of Geophysics &  
Planetary Physics  
Univ. of California, San Diego  
P.O. Box 109  
La Jolla, CA 92037

Mr. Edward Giller  
Pacific Seirra Research Corp.  
1401 Wilson Boulevard  
Arlington, VA 22209

Dr. Jeffrey W. Given  
Sierra Geophysics  
11255 Kirkland Way  
Kirkland, WA 98033

Rong Song Jih  
Teledyne Geotech  
314 Montgomery Street  
Alexandria, Virginia 22314

Professor F.K. Lamb  
University of Illinois at  
Urbana-Champaign  
Department of Physics  
1110 West Green Street  
Urbana, IL 61801

Dr. Arthur Lerner-Lam  
Lamont-Doherty Geological Observatory  
of Columbia University  
Palisades, NY 10964

Dr. L. Timothy Long  
School of Geophysical Sciences  
Georgia Institute of Technology  
Atlanta, GA 30332

Dr. Peter Malin  
University of California at Santa Barbara  
Institute for Central Studies  
Santa Barbara, CA 93106

Dr. George R. Mellman  
Sierra Geophysics  
11255 Kirkland Way  
Kirkland, WA 98033

Dr. Bernard Minster  
Institute of Geophysics and Planetary  
Physics, A-205  
Scripps Institute of Oceanography  
Univ. of California, San Diego  
La Jolla, CA 92093

Professor John Nabelek  
College of Oceanography  
Oregon State University  
Corvallis, OR 97331

Dr. Geza Nagy  
U. California, San Diego  
Dept of Ames, M.S. B-010  
La Jolla, CA 92093

Dr. Jack Oliver  
Department of Geology  
Cornell University  
Ithaca, NY 14850

Dr. Robert Phinney/Dr. F.A. Dahlen  
Dept of Geological  
Geophysical Sci. University  
Princeton University  
Princeton, NJ 08540 (2 copies)

RADIX Systems, Inc.  
Attn: Dr. Jay Pulli  
2 Taft Court, Suite 203  
Rockville, Maryland 20850

Dr. Norton Rimer  
S-CUBED  
A Division of Maxwell Laboratory  
P.O. 1620  
La Jolla, CA 92038-1620

Professor Larry J. Ruff  
Department of Geological Sciences  
1006 C.C. Little Building  
University of Michigan  
Ann Arbor, MI 48109-1063

Dr. Richard Sailor  
TASC Inc.  
55 Walkers Brook Drive  
Reading, MA 01867

Thomas J. Sereno, Jr.  
Service Application Int'l Corp.  
10210 Campus Point Drive  
San Diego, CA 92121

Dr. David G. Simpson  
Lamont-Doherty Geological Observ.  
of Columbia University  
Palisades, NY 10964

Dr. Bob Smith  
Department of Geophysics  
University of Utah  
1400 East 2nd South  
Salt Lake City, UT 84112

Dr. S. W. Smith  
Geophysics Program  
University of Washington  
Seattle, WA 98195

Dr. Stewart Smith  
IRIS Inc.  
1616 N. Fort Myer Drive  
Suite 1440  
Arlington, VA 22209

Rondout Associates  
ATTN: Dr. George Sutton,  
Dr. Jerry Carter, Dr. Paul Pomeroy  
P.O. Box 224  
Stone Ridge, NY 12484 (4 copies)

Dr. L. Sykes  
Lamont Doherty Geological Observ.  
Columbia University  
Palisades, NY 10964

Dr. Pradeep Talwani  
Department of Geological Sciences  
University of South Carolina  
Columbia, SC 29208

Dr. R. B. Tittmann  
Rockwell International Science Center  
1049 Camino Dos Rios  
P.O. Box 1085  
Thousand Oaks, CA 91360

Professor John H. Woodhouse  
Hoffman Laboratory  
Harvard University  
20 Oxford St.  
Cambridge, MA 02138

Dr. Gregory B. Young  
ENSCO, Inc.  
5400 Port Royal Road  
Springfield, VA 22151-2388

OTHERS (FOREIGN)

Dr. Peter Basham  
Earth Physics Branch  
Geological Survey of Canada  
1 Observatory Crescent  
Ottawa, Ontario  
CANADA K1A 0Y3

Dr. Eduard Berg  
Institute of Geophysics  
University of Hawaii  
Honolulu, HI 96822

Dr. Michel Bouchon - Universite  
Scientifique et Medicale de Grenob  
Lab de Geophysique - Interne et  
Tectonophysique - I.R.I.G.M-B.P.  
38402 St. Martin D'Herès  
Cedex FRANCE

Dr. Hilmar Bungum/NTNF/NORSAR  
P.O. Box 51  
Norwegian Council of Science,  
Industry and Research, NORSAR  
N-2007 Kjeller, NORWAY

Dr. Michel Campillo  
I.R.I.G.M.-B.P. 68  
38402 St. Martin D'Herès  
Cedex, FRANCE

Dr. Kin-Yip Chun  
Geophysics Division  
Physics Department  
University of Toronto  
Ontario, CANADA M5S 1A7

Dr. Alan Douglas  
Ministry of Defense  
Blacknest, Brimpton,  
Reading RG7-4RS  
UNITED KINGDOM

Dr. Manfred Henger  
Fed. Inst. For Geosciences & Nat'l Res.  
Postfach 510153  
D-3000 Hannover 51  
FEDERAL REPUBLIC OF GERMANY

Dr. E. Husebye  
NTNF/NORSAR  
P.O. Box 51  
N-2007 Kjeller, NORWAY

Ms. Eva Johannisson  
Senior Research Officer  
National Defense Research Inst.  
P.O. Box 27322  
S-102 54 Stockholm  
SWEDEN

Tormod Kvaerna  
NTNF/NORSAR  
P.O. Box 51  
N-2007 Kjeller, NORWAY

Mr. Peter Marshall, Procurement  
Executive, Ministry of Defense  
Blacknest, Brimpton,  
Reading FG7-4RS  
UNITED KINGDOM (3 copies)

Dr. Ben Menaheim  
Weizman Institute of Science  
Rehovot, ISRAEL 951729

Dr. Svein Mykkeltveit  
NTNF/NORSAR  
P.O. Box 51  
N-2007 Kjeller, NORWAY (3 copies)

Dr. Robert North  
Geophysics Division  
Geological Survey of Canada  
1 Observatory crescent  
Ottawa, Ontario  
CANADA, K1A 0Y3

Dr. Frode Ringdal  
NTNF/NORSAR  
P.O. Box 51  
N-2007 Kjeller, NORWAY

Dr. Jorg Schlittenhardt  
Federal Inst. for Geosciences & Nat'l Res.  
Postfach 510153  
D-3000 Hannover 51  
FEDERAL REPUBLIC OF GERMANY

University of Hawaii  
Institute of Geophysics  
ATTN: Dr. Daniel Walker  
Honolulu, HI 96822

FOREIGN CONTRACTORS

Dr. Ramon Cabre, S.J.  
c/o Mr. Ralph Buck  
Economic Consular  
American Embassy  
APO Miami, Florida 34032

Professor Peter Harjes  
Institute for Geophysik  
Rhur University/Bochum  
P.O. Box 102148, 4630 Bochum 1  
FEDERAL REPUBLIC OF GERMANY

Professor Brian L.N. Kennett  
Research School of Earth Sciences  
Institute of Advanced Studies  
G.P.O. Box 4  
Canberra 2601  
AUSTRALIA

Dr. B. Massinon  
Societe Radiomana  
27, Rue Claude Bernard  
7,005, Paris, FRANCE (2 copies)

Dr. Pierre Mechler  
Societe Radiomana  
27, Rue Claude Bernard  
75005, Paris, FRANCE

GOVERNMENT

Dr. Ralph Alewine III  
DARPA/NMRO  
1400 Wilson Boulevard  
Arlington, VA 22209-2308

Dr. Robert Blandford  
DARPA/NMRO  
1400 Wilson Boulevard  
Arlington, VA 22209-2308

Sandia National Laboratory  
ATTN: Dr. H. B. Durham  
Albuquerque, NM 87185

Dr. Jack Evernden  
USGS-Earthquake Studies  
345 Middlefield Road  
Menlo Park, CA 94025

U.S. Geological Survey  
ATTN: Dr. T. Hanks  
Nat'l Earthquake Resch Center  
345 Middlefield Road  
Menlo Park, CA 94025

Dr. James Hannon  
Lawrence Livermore Nat'l Lab.  
P.O. Box 808  
Livermore, CA 94550

Paul Johnson  
ESS-4, Mail Stop J979  
Los Alamos National Laboratory  
Los Alamos, NM 87545

Ms. Ann Kerr  
DARPA/NMRO  
1400 Wilson Boulevard  
Arlington, VA 22209-2308

Dr. Max Koontz  
US Dept of Energy/DP 5  
Forrestal Building  
1000 Independence Ave.  
Washington, D.C. 20585

Dr. W. H. K. Lee  
USGS  
Office of Earthquakes, Volcanoes,  
& Engineering  
Branch of Seismology  
345 Middlefield Rd  
Menlo Park, CA 94025

Dr. William Leith  
USGS  
Mail Stop 928  
Reston, VA 22092

Dr. Richard Lewis  
Dir. Earthquake Engineering and  
Geophysics  
U.S. Army Corps of Engineers  
Box 631  
Vicksburg, MS 39180

Dr. Robert Masse'  
Box 25046, Mail Stop 967  
Denver Federal Center  
Denver, Colorado 80225

Richard Morrow  
ACDA/VI  
Room 5741  
320 21st Street N.W.  
Washington, D.C. 20451

Dr. Keith K. Nakanishi  
Lawrence Livermore National Laboratory  
P.O. Box 808, L-205  
Livermore, CA 94550 (2 copies)

Dr. Carl Newton  
Los Alamos National Lab.  
P.O. Box 1663  
Mail Stop C335, Group E553  
Los Alamos, NM 87545

Dr. Kenneth H. Olsen  
Los Alamos Scientific Lab.  
Post Office Box 1663  
Los Alamos, NM 87545

Howard J. Patton  
Lawrence Livermore National  
Laboratory  
P.O. Box 808, L-205  
Livermore, CA 94550

Mr. Chris Paine  
Office of Senator Kennedy  
SR 315  
United States Senate  
Washington, D.C. 20510

AFOSR/NP  
ATTN: Colonel Jerry J. Perrizo  
Bldg 410  
Bolling AFB, Wash D.C. 20332-6448

HQ AFTAC/TT  
Attn: Dr. Frank F. Pilotte  
Patrick AFB, Florida 32925-6001

Mr. Jack Rachlin  
USGS - Geology, Rm 3 C136  
Mail Stop 928 National Center  
Reston, VA 22092

Robert Reinke  
AFWL/NTESG  
Kirtland AFB, NM 87117-6008

HQ AFTAC/TGR  
Attn: Dr. George H. Rothe  
Patrick AFB, Florida 32925-6001

Donald L. Springer  
Lawrence Livermore National Laboratory  
P.O. Box 808, L-205  
Livermore, CA 94550

Dr. Lawrence Turnbull  
OSWR/NED  
Central Intelligence Agency  
CIA, Room 5G48  
Washington, D.C. 20505

Dr. Thomas Weaver  
Los Alamos Scientific Laboratory  
Los Alamos, NM 97544

AFGL/SULL  
Research Library  
Hanscom AFB, MA 01731-5000 (2 copies)

Secretary of the Air Force (SAFRD)  
Washington, DC 20330  
Office of the Secretary Defense  
DDR & E  
Washington, DC 20330

HQ DNA  
ATTN: Technical Library  
Washington, DC 20305

DARPA/RMO/RETRIEVAL  
1400 Wilson Blvd.  
Arlington, VA 22209

DARPA/RMO/Security Office  
1400 Wilson Blvd.  
Arlington, VA 22209

AFGL/XO  
Hanscom AFB, MA 01731-5000

AFGL/LW  
Hanscom AFB, MA 01731-5000

DARPA/PM  
1400 Wilson Boulevard  
Arlington, VA 22209

Defense Technical  
Information Center  
Cameron Station  
Alexandria, VA 22314  
(5 copies)

Defense Intelligence Agency  
Directorate for Scientific &  
Technical Intelligence  
Washington, D.C. 20301

Defense Nuclear Agency/SPSS  
ATTN: Dr. Michael Shore  
6801 Telegraph Road  
Alexandria, VA 22310

AFTAC/CA (STINFO)  
Patrick AFB, FL 32925-6001

Dr. Gregory van der Vink  
Congress of the United States  
Office of Technology Assessment  
Washington, D.C. 20510

Mr. Alfred Lieberman  
ACDA/VI-OA'State Department Building  
Room 5726  
320 - 21st Street, NW  
Washington, D.C. 20451

TACTEC  
Battelle Memorial Institute  
505 King Avenue  
Columbus, OH 43201 (Final report only)